CHALMERS
UNIVERSITY OF TECHNOLOGY

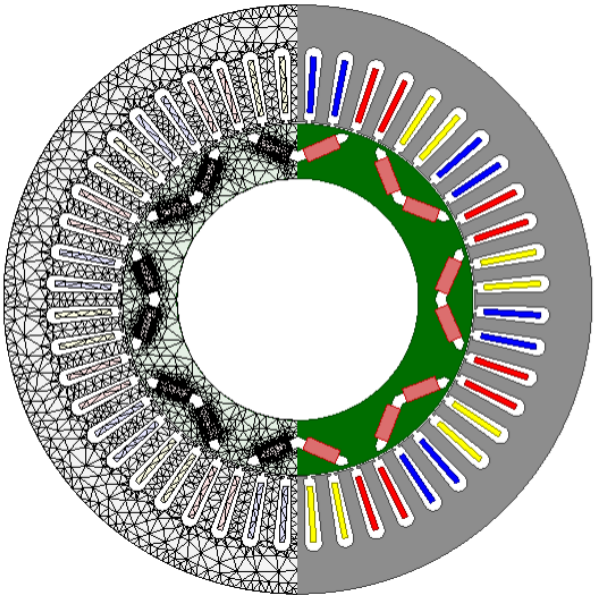

Torque ripple optimization for Electric Drive Modules with Current Harmonic Injection method

Master's thesis in Electric power engineering

EHSAN BAHMANI
SIMA SOLTANIPOUR

Department of Electrical Engineering
CHALMERS UNIVERSITY OF TECHNOLOGY
Gothenburg, Sweden 2018

Master's thesis 2018

Torque ripple optimization for Electric Drive Modules with Current Harmonic Injection method

EHSAN BAHMANI
SIMA SOLTANIPOUR

CHALMERS
UNIVERSITY OF TECHNOLOGY

Department of Electrical Engineering
Division of Electric Power Engineering
Chalmers University of Technology
Gothenburg, Sweden 2018

Torque ripple optimization for Electric Drive Modules with Current Harmonic Injection method
EHSAN BAHMANI
SIMA SOLTANIPOUR

Supervisor: Alexandra Nafari, BorgWarner
Examiner: Torbjorn Thiringer,Chalmers University of Technology, Department of Electrical Engineering

Master's Thesis 2018
Department of Electrical Engineering
Division of Electric Power Engineering
Chalmers University of Technology
SE-412 96 Gothenburg
Telephone +46 31 772 1000

Cover: Three phase Permenant Magnet Synchronous Motor 2D model by Finite Element Methods.

Typeset in LaTeX
Printed by Chalmers liberary, Reproservice
Gothenburg, Sweden 2018

Torque ripple optimization for Electric Drive Modules with Current Harmonic Injection method.

EHSAN BAHMANI
SIMA SOLTANIPOUR
Department of Energy and Environment
Chalmers University of Technology

Abstract

In recent years, the Noise, Vibration and Harshness (NVH) issue in HEVs and EVs is becoming a considerable concern in the automotive industry. In the absence of a combustion engine in EVs and shrinked size of the engine in HEVs, one of the main sources of NVH especially in lower speeds, is torque ripple of electric motors. Torque ripple is mainly generated due to undesired harmonics in the back-ElectroMagnetic Force (EMF), current harmonics, cogging torque and high frequency harmonics due to inverter switching and slot opening. To suppress the harmonics, different methods have been investigated and implemented in the literature. Most methods deals with the geometrical design of PMSMs which consequently introduce, a high cost of manufacturing. This thesis is dedicated to torque ripple optimization using current harmonic injection. In this methodology, harmonics are added to the reference current signal to define a new inverter output current. To investigate the applicability of the mentioned method, the formation of the electromagnetic fluxes and forces in the air gap of an IPMSM are investigated further. In addition, the analytical calculation of the electromagnetic torque from the tangential forces acting on the air gap line is presented.

This thesis work has been conducted on an existing Permanent Magnet Synchronous Motor (PMSM) model. The motor has been modelled by a Finite Element Analysis (FEA) based software and investigated in several operating points. It is shown that the torque ripple is reduced by 73 % in average. A disadvantage that has to be mentioned is that a 20 % increase in core losses is observed after injecting current harmonics which is not desired.

Keywords: Permanent Magnet Synchronous Motors (PMSMs), Electric Vehicles (EVs), Hybrid Electric Vehicles (HEVs), Noise, Vibration and Harshness (NVH), Torque ripple optimization, Current harmonic injection, Maxwell Stress Tensor.

Acknowledgements

This work has been carried out at the Department of Energy and Environment of Chalmers university of technology and BorgWarner. The project is affiliated by BorgWarner Company.

We would like to express our sincere gratitude to Alexandra Nafari our industrial supervisor at BorgWarner company for her valuable and consistence guidance, motivation and support on the way. Her encouragement, insightful comments helped us to move forward and get a better understanding of the case in industry.

Furthermore, we would like to thank our advisor Prof.Torbjörn Thiringer for the continuous support of our study and research, for his patience, enthusiasm, and immense knowledge. His guidance helped us in all the time of research and writing of this thesis.

Besides our advisers, we would like to thank Amin Bahmani and all the people of the Electric Power Engineering division at Chalmers and BorgWarner who have willingly shared their knowledge and precious time to help us throughout this work.

Last but not the least, we would like to express our love to our families for the everlasting love and support in our lives which made us to who we are.

Ehsan Bahmani
Sima Soltanipour
Gothenburg, Sweden
August, 2018

List of Abbreviation

AC ..... Alternating Current
DC ..... Direct Current
dq ..... Direct and Quadrant
DTC ..... Direct Torque Control
EMF ..... ElectroMagnetic Force
EV ..... Electric Vehicle
FEA ..... Finite Element Analysis
FEM ..... Finite Element Method
FFT ..... Fast Fourier Transform
FOC ..... Field Oriented Control
GHGs ..... Green House Gases
HEV ..... Hybrid Electric Vehicle
IPM ..... Interior Permanent Magnet
IPMSM ..... Interior Permanent Magnet Synchronous Motor
MMF ..... MagnetoMotive Force
MTPA ..... Maximum Torque Per Amper
NVH ..... Noise, Vibration and Harshness
PM ..... Permanent Magnet
PMSM ..... Permanent Magnet Synchronous Motor
PWM ..... Pulse Width Modulation
RMS ..... Root Mean Square
RPM ..... Revolution Per Minute
SPMSM ..... Surface Permanent Magnet Synchronous Motor
VSI ..... Voltage Source Inverter

Ehsan Bahmani - Sima Soltanipour
Gothenburg, Sweden
June, 2018

Contents

1

Introduction

1.1 Problem Background

Nowadays, new legislations are being proposed by govenments throughout the world to decrease Green House Gases (GHGs) emission. Hence, the tendency towards Electric Vehicle (EVs) and Hybrid Electric Vehicles (HEVs) which generate less pollution, has been increased significantly. Permanent Magnet Synchronous Motors (PMSMs) are one of the most desired motors in a wide range of EVs and HEVs due to their inherent characteristics such as small size, high torque density, low rotor inertia, high efficiency, and high power density [17].

In recent years, the Noise, Vibration and Harshness (NVH) issue in HEVs and EVs has become more and more important. The NVH sources in the electric vehicle can be classified as aerodynamical: like wind and cooling fans, mechanical: such as engine, brake, tire contact patch, and road surface or it can originate from electrical parts like electromagnetically-excited acoustic noise and vibrations from actuators, the traction motor and etc.

As an electrical source of NVH in PMSMs, torque ripple is of a great interest which is caused mainly by undesired harmonics generated by non-ideal back ElectroMotive Force (EMF) and current and cogging torque. On the other hand, the electromagnetic source of torque ripple in the PMSMs is a result of complex interaction of stator and rotor flux intensity and permeance variation of their magnetic circuits [2]. For suppression of the NVH caused by torque ripple of traction motors in HEVs and EVs a wide range of method has been studied and implemented in previous works which will be shortly discussed in the following.

1.2 Previous work

To improve torque ripple in traction motors, different approaches either in machine design perspective or control strategies have been investigated and implemented in

many studies. In [12, 13] the skewing of the rotor magnet in a Switched Reluctance Permanent Magnet Synchronous Motor (SRPMSM) and a PMSM has been investigated respectively. Changes to rotor magnets such as adjusting the pole angles, pole pairing are defined as applicable methods to reduce the torque ripple in electric motors [14, 16]. In [15] an approach called the multi-slicing is implemented, using this methodology the motor's length is axially divided into several equal slices to reduce the torque ripple. These articles as well as several others with approaches toward mechanical design have successfully obtained reduction in torque ripple. However, the high cost and complexity of manufacturing and designing, make these methods undesired. There are other studies focusing on controlling methods to decrease current harmonics generated by the nonlinear characteristic of the switches in the inverter such as dead-time [11] and voltage drop while some of the others are non-dead time control [7], voltage compensation [8] and time compensation [9] which have some drawbacks such as additional hardware, complex control strategy [10], etc.

1.3 Purpose of the thesis and contributions

This thesis work aims to investigate the effect of current harmonic injection on torque harmonics and effectiveness of the proposed compensation algorithm on torque ripple by considering dominant back EMF harmonics. To be able to analyze the results and understand the sources behind harmonic generation in current, back EMF and consequently torque, flux density and force density in the air gap are studied and presented. In this study, several operating points at different speeds and torques are investigated and the target is to reduce torque ripple as much as possible.

1.4 Thesis outline

In chapter 2 essential theories to help the understanding of an electric drive system and inverter working principle as well as modelling have been covered. Besides, the equivalent circuit and related analytical expression for PMSMs are presented. The speed and current Field Oriented Controller (FOC) for the motor along with Maximum Torque Per Ampere (MTPA) and Pulse Width Modulation (PWM) techniques are discussed in details. Chapter 3 focuses on defining torque ripple sources like cogging torque, harmonics of the back EMF and current and it also describe the compensation algorithm used in this project in details. The theoretical aspects introduced by the implementation of this method is also discussed in this chapter.

Chapter 4 presents the modelling procedure of the IPMSM in the Finite Element (FE) based software ANSYS Maxwell in 2D and the requirements for this analysis. Chapter 5 is assigned to investigate the electromagnetic source of torque by analyzing the flux and force density in the air gap. Finally, in chapter 6 the results obtained from simulations are studied and compared with analytical results and the conclusion is presented in chapter 7.

2

Electric Drive System

An electric motor for Hybrid and fully electric vehicles for traction applications can be chosen based on the qualitative features such as cost and performance. In terms of performance, traction motors must have a high efficiency, high power and torque density across a wide range of speed, a high power to weight ratio is also of interest in these motors [20]. A broad range of investigations on motor topology are done in [21] on different motors such as PMSMs, induction machines and synchronous reluctance machines by specifying relative qualitative indices to each topology. The best suited machine type concluded from this study is the interior permanent magnet machine which can provide a high torque density and moderate high-speed performance. However, the cost of these machines is relatively high. IPMSMs not only use the magnetic torque but also reluctance torque which add to the magnetic torque and increase the total torque. IPMs have good overload and field weakening capabilities.

The selected topology for conducting the simulation and studies in the presented work is an IPMSM machine due to its range of production in the automotive industry. The thesis work is based on a V type single layer magnet IPMSM.
In this chapter, the electric drive system, PMSMs modeling in Direct and Quadrant (dq) axis rotor reference frame is presented along with the inverter and current controller working principle in details.

2.1 PMSM equivalent circuit

PMSMs are typically modelled in the dq-axis reference frame fixed to the rotor for speed-torque predicting. The stator voltages relation with phase currents of the PMSM in the rotor reference frame can be expressed as

$$u_{sd} = L_{sd}\frac{di_{sd}}{dt} - \omega_r L_{sq} i_{sq} + R_s i_{sd} \tag{2.1}$$

$$u_{sq} = L_{sq}\frac{di_{sq}}{dt} + \omega_r L_{sd} i_{sd} + R_s i_{sq} + \omega_r \Psi_m \tag{2.2}$$

where, u_{sd} is the stator voltage in direct axis while u_{sq} is stator voltage in quadrant direction, i_{sd} and i_{sq} are stator currents and L_{sd}, L_{sq} are the stator inductance in direct and quadratic direction respectively, R_s is stator resistance, ω_r is the rotor electrical speed and Ψ_m is the flux linkage generated by the permanent magnets. The presented model only include ideal components without considering any non-linearity due to harmonics in induced voltage. Fig 2.1 is the equivalent circuit of a PMSM decoupled in direct and quadratic direction corresponding to the above equations.

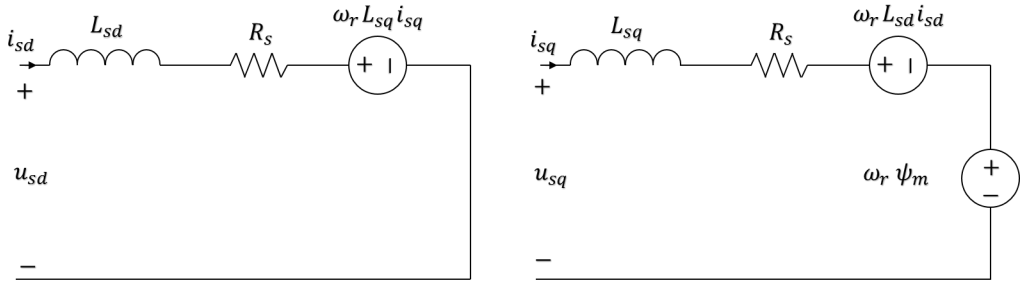

Figure 2.1: Equivalent circuit of PMSM in dq-axis rotor reference frame

The flux linkage components relation with inductance and current can be expressed as

$$\Psi_{sd} = L_{sd} i_{sd} + \Psi_m \tag{2.3}$$

$$\Psi_{sq} = L_{sq} i_{sq} \tag{2.4}$$

$$|\Psi_s| = \sqrt{\Psi_{sd}^2 + \Psi_{sq}^2} \tag{2.5}$$

The electromagnetic torque is defined by the equation,

$$T_e = \frac{3n_p}{2}(\Psi_d i_{sd} - \Psi_q i_{sd}) \tag{2.6}$$

where n_p is the number of pole pairs in the rotor.

As L_{sd} and L_{sq} depends on both current in direct and quadratic directions they vary as the currents vary. So as to consider the real model of the motor this variation in parameters is also taken into account. On the other hand, the path in q-direction can be saturated easier so L_{sq} usually changes more than L_{sd} [17] [22]

2.2 Three-phase two level inverter

DC power can be transferred to the AC power with desired voltage and frequency by a power electronic device called inverter. There are many aspects in which inverters

can be classified into, one way is to categorize them based on number of levels i.e. two level or multilevel inverters. The main advantages of using multilevel inverters are lower switching losses due to the fact that lower switching frequency with minimum harmonic distortions for the same switching frequency can be used. However, this type of inverter has more switches which increases cost and it is thus more complex to control. Furthermore, multilevel inverters might increase losses in the battery of the car in some operation points due to different harmonic current contents [2]. A two-level inverter operates with Pulse Width Modulation (PWM) strategy which is explained in the next section. A two level inverter uses DC voltage from the battery of the vehicle and transforms it to three-phase AC voltage to generate the rotating field and produce torque for the PMSM. As can be seen from Fig.2.2 a three-phase two-level inverter includes six switches which are arranged in three phase legs and there is one free-wheeling diode in parallel for each switch. In this thesis work, the impact of inverter and the modulation technique used for switching on torque ripple is not studied. Therefore, it is assumed that inverter is working ideally and cause no non-linearity in the back EMF and current waveform.

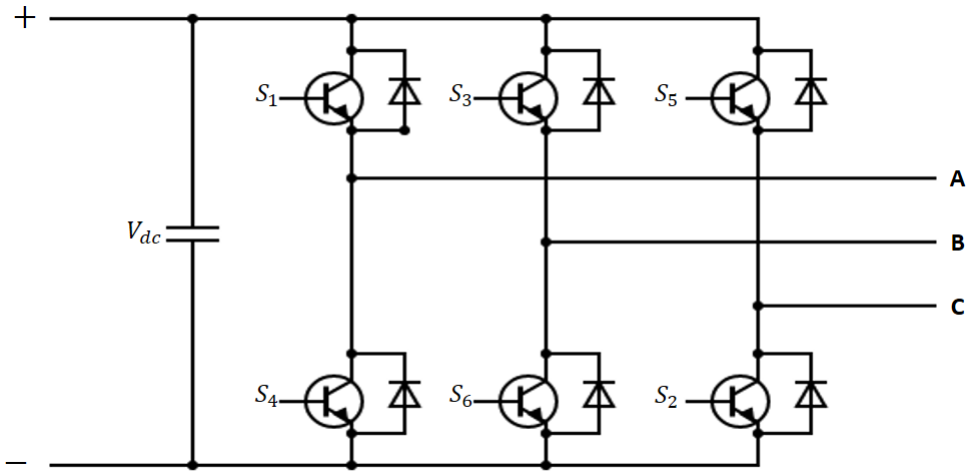

Figure 2.2: Three-phase two-level inverter

2.3 Pulse width modulation (PWM)

PWM is a method of generating signals in order to control the voltage and thus amount of power which is transferred to the external device such as a motor. In general, the aim of the PWM strategy is to achieve a symmetrical three phase sine voltage waveform. As can be seen from Fig.2.3 three reference sine waves for each phase is compared with a triangular wave in such a way that when the reference wave is higher than the triangular wave in the corresponding leg, the upper switch

is on and the bottom switch is off. On the other hand, when the reference wave is lower than the triangular wave in the corresponding leg, the upper switch is off and the bottom switch is on.

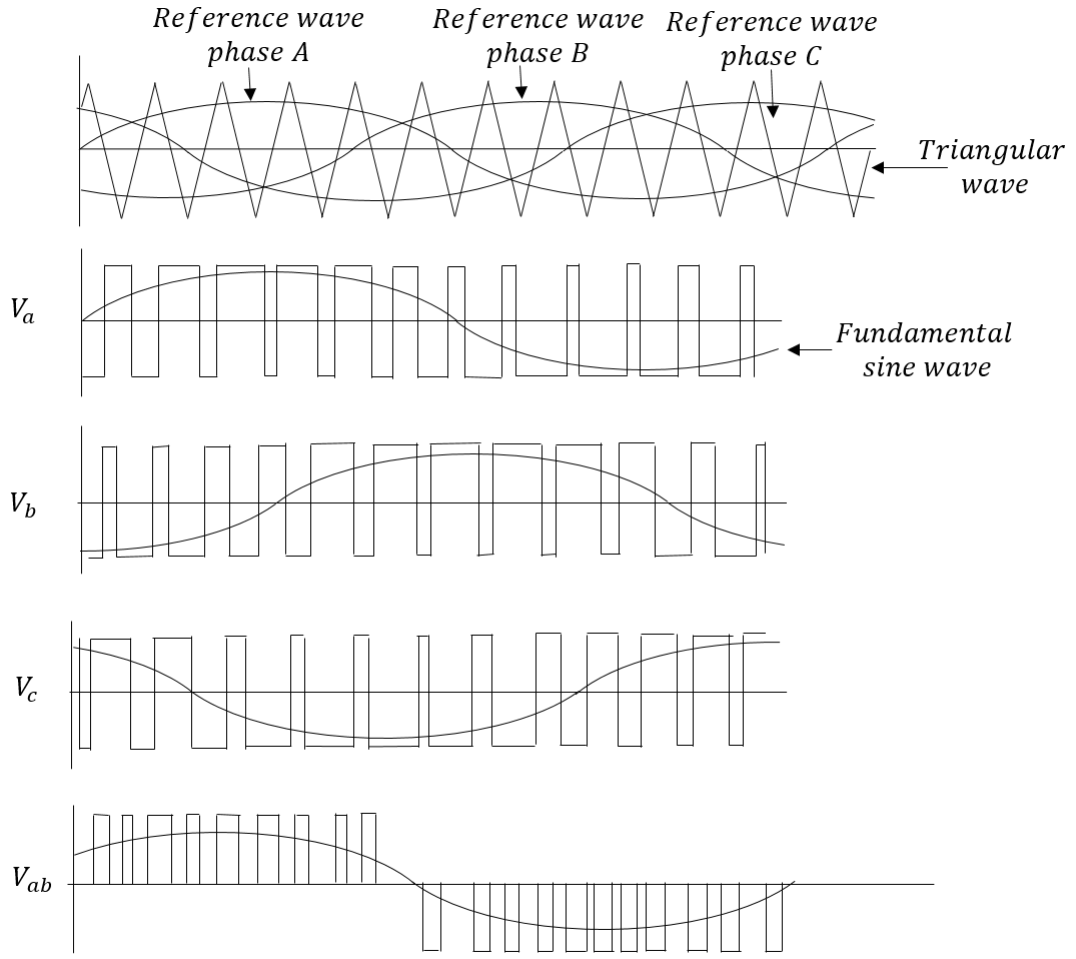

Figure 2.3: PWM waveform include reference sine wave, triangular wave and generated wave

The amplitude of the output voltage or current depends on the duty cycle. By increasing the on time of the switches the output power is increased and by decreasing it the output power is decreased.

2.4 PMSM Controller

The goal of any machine controller is to keep the desired speed of the motor constant. To achieve this goal the produced torque has to be controlled. The electromagnetic

torque equation of the PMSM is commonly expressed as

$$T_e = \frac{3n_p}{2}(\Psi_m i_{sq}) + \frac{3n_p}{2}(L_{sd} - L_{sq})i_{sd}i_{sq} \tag{2.7}$$

where n_p is the number of pole pairs.

It can be concluded from (2.7) that the electromagnetic torque in a PMSM includes two parts, the first part is called excitation torque and it is formed due to the interaction between i_{sq} and Ψ_m and the second term is called reluctance torque and it is formed due to the saliency of the rotor.
In non-salient motors, $L_d = L_q$ so the electromagnetic torque can be written as

$$T_e = \frac{3n_p}{2}(\Psi_m i_{sq}) \tag{2.8}$$

2.4.1 Field oriented control

The are many machine control methods used in industry but in this work a Field Oriented Control (FOC) is studied. In this type of controller a current loop to control the electromagnetic torque is implemented along with a feedback of the speed. By using the FOC, it is possible to operate the motor at its optimum torque and speed at any time. Fig.2.4 shows a schematic model of the FOC. The area enclosed by a red rectangle area shows a normal field oriented controller and the shaded area shows an addition to the controller which generates harmonics that will be added to the current. The intentionally added harmonics cancel out the effect of already existing harmonics in the current and back EMF so with the new reference values for currents in the dq direction the torque ripple will be reduced.

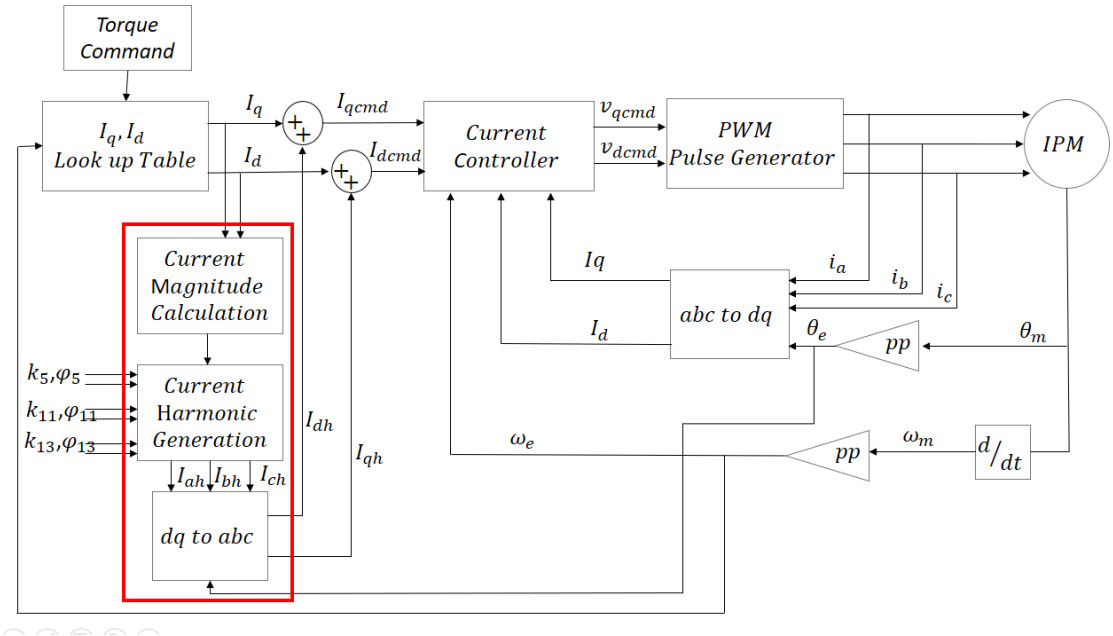

Figure 2.4: Field oriented controller

In a field oriented controller the produced torque is controlled by the stator current i_s. The strategy of this controller is realized in the rotating dq reference frame. The currents in dq-axis are expressed as

$$i_{sd} = \frac{1}{L_{sd}s + R_s}(u_{sd} + \omega_r L_{sq} i_{sq}) \tag{2.9}$$

$$i_{sq} = \frac{1}{L_{sq}s + R_s}(u_{sq} - \omega_r L_{sd} i_{sd} - \omega_r \Psi_m) \tag{2.10}$$

where i_{sd} and i_{sq} are stator current components in direct and quadrant direction so $i_s = i_{sd} + i_{sq}$. ψ_m is the flux linkage caused by the permanent magnets.

To implement a closed loop controller, the rotor position in mechanical degrees is measured and transformed to the rotor position in electrical degrees. The three phase current of the motor is measured and fed back to the current controller. By using Clarke and Park transformation, two phase currents I_d and I_q can be found. At the same time, in order to control the rotor speed, another loop is used to measure the rotor speed and then it is compared with the desired speed. The difference between them, i.e. an error signal is fed to the speed regulator and then the speed regulator creates a torque command which is fed to a look up table to form the reference values of $I_{d_{ref}}$ and $I_{q_{ref}}$ are obtained based on one of these strategies:

1. Constant torque angle control
2. Unity power factor control
3. Maximum torque per amper (MTPA)
4. Constant stator flux control

2.4.2 Maximum torque per amper MTPA

The MTPA strategy works in such a way that for a required torque, the minimum current is used in order to minimize copper losses and increase the overall efficiency of the motor. The concept of MTPA can be realized by Fig.2.6.

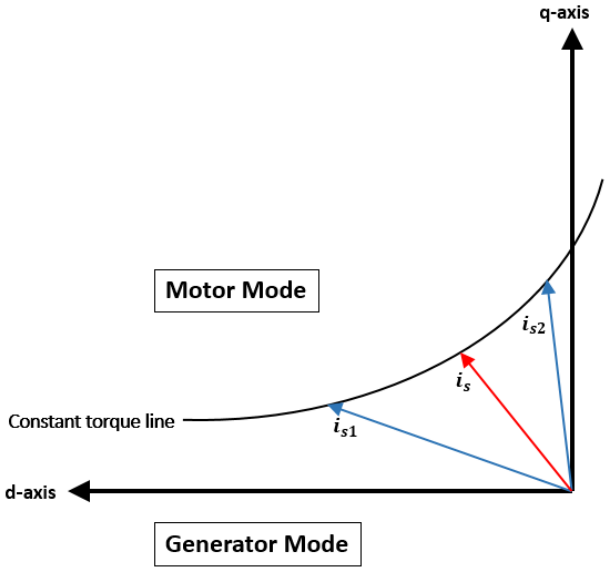

Figure 2.5: Vectors which show the minimum current for a given torque in a IPMSM

As can be seen from Fig.2.6 for a given torque there are several possibilities for stator currents i_s,i_{s_1} and i_{s_2}. The minimum value of the current is related to the i_s vector that can produce the desired torque. The MTPA curve can be made by connecting all the intersection points of minimum current vectors with the corresponding torque. In order to make the MTPA curve for an IPMSM, the electromagnetic torque equation and limitation of stator current equation must be considered. The stator current in quadrant direction limited to maximum current is expressed as

$$i_{s_{max}}^2 = i_{sd}^2 + i_{sq}^2 \tag{2.11}$$

$$i_{sq} = \sqrt{i_{s_{max}}^2 - i_{sd}^2} \tag{2.12}$$

where $i^2_{s_{max}}$ is the maximum current amplitude of the stator which is fed to the IPMSM by the inverter.
By substituting i_{sq} from (2.12) into (2.7), electromagnetic toque expression can be rewritten as

$$T_e = \frac{3n_p}{2}(\Psi_m\sqrt{i^2_{s_{max}} + i^2_{s_d}}) + \frac{3n_p}{2}(L_{sd} - L_{sq})i_{sd}\sqrt{i^2_{s_{max}} + i^2_{s_d}} \tag{2.13}$$

In order to find the minimum value of i_{sd} which can produce the desired torque, derivation of T_e is calculated with respect to i_{sd} as can be seen in the following equation

$$\frac{\mathrm{dT_e}}{\mathrm{d}i_{s_d}} = \frac{3n_p}{2}\frac{-i_{sd}\psi_m + (L_{sd} - L_{sq})(i_{smax} - 2i^2_{sd})}{\sqrt{i^2_{s_{max}} + i^2_{sd}}} \tag{2.14}$$

By putting (2.14) equal to zero, the minimum i_{sd} which corresponds to the desired torque can be obtained as

$$2i^2_{sd} + \frac{\psi_m}{L_{sd} - L_{sq}}.i_{sd} - i^2_{s_{max}} = 0 \tag{2.15}$$

$$i_{sd} = \frac{-\psi_m + \sqrt{\psi^2_m + 8(L_{sd} - L_{sq})^2 i^2_{s_{max}}}}{4(L_{sd} - L_{sq})} \tag{2.16}$$

By having equations (2.7), (2.12), (2.16) the MTPA curve of the IPMSM can be obtained and it can be concluded that the MTPA is dependent on the motor parameters like flux linkage of the permanent magnet and also the d and q axis inductances.

3

Torque pulsation in IPMSMs

As mentioned earlier, one of the drawbacks of IPMSMs is noise and vibration caused by torque ripples. This thesis is mainly focused on the torque ripple minimization, thus reasons for generation of ripple in their torque needs to be identified. Torque in an IPMSM can be generated by Lorentz torque which generates the work torque called reluctance torque created by the reluctance difference in d and q direction and cogging torque. Torque ripple is caused due to the distortion of flux density distribution in the air gap. Reluctance torque which appears in the salient electric motors with high saliency ratio can cause torque ripple due to different inductance (L_d , L_q) and also the cogging torque, a periodic oscillation, is due to interaction of rotating rotor and stator slots even though there is no current in the windings. [1, 13]

3.1 Cogging torque

The total magnetic field co-energy in a PMSM is expressed as

$$W_c = \frac{1}{2}Li^2 + \frac{1}{2}(R + R_m)\phi_m^2 + Ni\phi_m \tag{3.1}$$

where R and R_m are the reluctances seen by the Magnetomotive Force (MMF) source and magnetic force, ϕ_m is the magnetic flux between the magnets and the exciting coil. The torque can be calculated from the differentiation of the co-energy with respect to the mechanical angle which is illustrated by

$$T = \frac{\partial W_c}{\partial \theta}|_{i=constant} \tag{3.2}$$

Consequently, the torque can be written as

$$T = \frac{1}{2}i^2\frac{dL}{d\theta} - \frac{1}{2}\phi_m^2\frac{dR}{d\theta} + Ni\frac{d\phi_m}{d\theta} \tag{3.3}$$

where $L = N^2/R_m$ is a constant value, not varying with the rotating position θ so the first term in (3.3) becomes zero. In case of no excitation current in the winding,

the third term will be zero as well and the torque is only produced by the second term which is proportional to the square of the magnetic flux. Thus, the cogging torque can be expressed by only focusing on the magnetic interaction along with reluctance change between the stator teeth and magnet according to

$$T_{cog} = -\frac{1}{2}\phi_m^2 \frac{dR}{d\theta} \tag{3.4}$$

It can be seen that cogging torque is determined by air gap flux and reluctance variation in the magnetic circuit with a rotating displacement so cogging torque is formed as the magnet flux travels through a changing reluctance. The cogging torque of a symmetrically structured PMSM is periodically distributed with respect to the mechanical angle[13]. Cogging torque exists and causes unsmooth motion even when the shaft is manually rotated.

3.2 Harmonics of current and Back-EMF in IPMSMs

Even in an ideal case when three phases of armature current waveforms are purely sinusoidal, non-linear loads always cause distortion. Linear loads have no effect on the current but nonlinear loads such as electric motors draw current in different shapes and make current waveforms quite complex. This complex waveform can be decomposed into a summation of several smaller sinusoidal waves according to the Fourier series formula. Harmonics are defined as a positive multiple of the fundamental frequency.[3]

In the IPMSM, one of the main reasons of torque ripple is current harmonics generated due to air gap magnetic field distortion, inverter voltage drop, dead time and etc. The back EMF of the permanent magnet synchronous motor also contains undesired harmonics which are only odd harmonics except for multiples of 3 due to the symmetry of the three-phase stator winding. It can be realized that the amplitude of the torque ripple is proportional to current and back EMF fundamental and harmonics components. Usually, the magnitude of the harmonics become lower by increasing the order of them. The three phases non-sinusoidal armature currents are expressed as

$$I_a = I_1 sin(\omega t + \theta) + \sum_u I_u sin\left(k_{iu} u\omega t + \beta_u\right) \tag{3.5}$$

$$I_b = I_1 sin(\omega t + \theta - \frac{2\Pi}{3}) + \sum_u I_u sin\left(k_{iu} u\omega t + \beta_u - \frac{2\Pi}{3}\right) \tag{3.6}$$

$$I_c = I_1 sin(\omega t + \theta + \frac{2\Pi}{3}) + \sum_u I_u sin\left(k_{iu} u\omega t + \beta_u + \frac{2\Pi}{3}\right) \tag{3.7}$$

where I_1 is the amplitude of current fundamental component, ω is the electrical angular velocity of the EM which is equal to ω=2πf , θ is the initial phase angle of the current fundamental component, I_u is the amplitude of the u_{th} harmonic component, u is the order of harmonic, β_u is the phase angle of the u_{th} current harmonic component and k_{iu} is a coefficient and its value is either 1 or -1 depending on the sequence (or direction) of the harmonics. The first term of the equations is the current fundamental component and the second term is the current harmonics. As can be seen from the above equations each phase has a 120 electrical degree shift towards other ones. Three phases non-sinusoidal back-EMFs are expressed as

$$E_a = E_1 sin(\omega t) + \sum_v E_v sin\left(k_{ev} v\omega t + \alpha_v\right) \tag{3.8}$$

$$E_a = E_1 sin(\omega t - \frac{2\Pi}{3}) + \sum_v E_v sin\left(k_{ev} v\omega t + \alpha_v - \frac{2\Pi}{3}\right) \tag{3.9}$$

$$E_a = E_1 sin(\omega t + \frac{2\Pi}{3}) + \sum_v E_v sin\left(k_{ev} v\omega t + \alpha_v + \frac{2\Pi}{3}\right) \tag{3.10}$$

where E_1 is the amplitude of the back-EMF fundamental component, ω is the electrical angular velocity of the EM, E_v is the amplitude of the v_{th} harmonic component, v is the order of harmonic, α_v is the phase angle of the v_{th} induced voltage harmonic component and k_{ev} is a coefficient and its value is either 1 or -1 depending on the sequence (or direction) of the harmonic.
The electromagnetic torque can be obtained from [3]

$$T_{em} = \frac{(E_A I_A + E_B I_B + E_C I_C)}{\omega} \tag{3.11}$$

where E_A, E_B and E_C are back-EMFs of phase A, B and C respectively, I_A, I_B and I_C are armature current of phase A, B and C respectively and ω is the angular velocity of the machine.

In order to have a constant torque, the current and back EMF wave forms need to be pure sinusoidal. It means that the input currents and back-EMF only contain the first term in the above equations, however it is impossible to have this condition for an IPMSM, even with purely sinusoidal input currents, the back EMF will contain different harmonics. It is due to different reluctance in the flux paths which will be discussed with more details in next sections. It can be shown by substituting (3.5), (3.6), (3.7), (3.8), (3.9) and (3.10) into (3.11), the electromagnetic torque will be divided into different parts($T_1 + T_2 + T_3 + T_4$) according to fundamental and harmonic components of armature current and back-EMF therefore

$$T_{em} = T_1 + T_2 + T_3 + T_4 \tag{3.12}$$

$$T_1 = \frac{3E_1 I_1}{2\omega} \cos(\theta) \tag{3.13}$$

$$T_2 = \frac{3E_v I_1}{2\omega} \sum_v \cos\left[(k_{ev}v - 1)\,\omega t + \theta - \alpha_v\right] \tag{3.14}$$

$$T_3 = \frac{3E_1 I_u}{2\omega} \sum_u \cos\left[(1 - k_{iu}u)\,\omega t + \beta_u\right] \tag{3.15}$$

$$T_4 = \frac{3E_v I_u}{2\omega} \sum_v \sum_u \cos\left[(k_{ev}v - k_{iu}u)\,\omega t + \beta_u - \alpha_v\right] \tag{3.16}$$

where;

- T_1 is the average torque which is generated by current and back-EMF fundamental components.
- T_2 is torque ripple which is generated by the fundamental component of armature current and harmonic components of the back-EMF.
- T_3 is torque ripple which is generated by the fundamental component of the back-EMF and harmonic components of the input current. T_2 and T_3 are torque ripple because $v, u \neq 1$.
- T_4 is generated by harmonic components of the back-EMF and current and the effect of it on the torque depends on $k_{ev}v$ and $k_{iu}u$, when $k_{ev}v \neq k_{iu}u$, T_4 appears as a ripple and causes torque pulsation, on the other hand when $k_{ev}v = k_{iu}u$, it appears as a constant value which affects the average torque and it is proportional to the harmonic components of the back-EMF and armature current, therefore by having the same order harmonics in the currents and back-EMF, the negative effect of T_4 on the torque will be eliminated. However the effect of T_4 on the average torque can be ignored because E_v and I_u are so small compared with the fundamental component.

It can be concluded that by having pure sinusoidal currents, T_3 and T_4 are zero but T_2 is not zero which causes torque ripple.

The harmonic order of the current and back-EMF wave can be expressed as $6k \pm 1$ for $k = 1, 2, 3, ...$ and it is $6k + 1$ when the coefficient is 1 and it is $6k - 1$ when the coefficient(harmonic sequence) is -1, therefore the back-EMF and armature current of phase a can be derived from (3.5) and (3.8) respectively

$$E_a = E_1 \sin\omega t + E_3 \sin 3\omega t + E_5 \sin 5\omega t + E_7 \sin 7\omega t + ... \tag{3.17}$$

$$I_a = I_1 \sin\omega t + I_5 \sin 5\omega t + I_7 \sin 7\omega t + I_{11} \sin 11\omega t + ... \tag{3.18}$$

E_n is produced by the n_{th} space harmonic of the air gap magnetic flux density B and I_n depends on input current harmonics. When the phase windings are connected

in delta, the PM flux-linkage and the resulting induced back-EMF contains high harmonics of order 3_{rd} and 9_{th}. The product of the back-EMF and current in one phase, which includes even order harmonics is proportional to the instantaneous torque generated by one phase. The result of adding the product of each phase together $(E_A I_A + E_B I_B + E_C I_C)$ will contain harmonics of the order of 6 and the other harmonics will be removed, therefore the instantaneous torque equation can be written as

$$T_{em} = T_0 + T_6 \cos(6\omega t) + T_{12} \cos(12\omega t) + T_{18} \cos(18\omega t) + ... \tag{3.19}$$

where T_0 is the average electromagnetic torque, T_6, T_{12} and T_{18}... are 6_{th}, 12_{th} and 18_{th} order of torque harmonics.

4

Finite element modeling of the machine

To validate the current harmonic injection method a 2D modeling of an Interior Permanent Magnet Synchronous Motor is done using the ANSYS software with the use of the electromagnetic suite. The motor specifications used to model the IPMSM is extracted from the data sheet of Toyota Prius 2004 car [19]. The design and technical data of the used IPMSM is illustrated in Table.4.1. The motor is modelled in 2D but in case of calculating torque the effective length of motor is needed, which is $L_e = 83.82$ mm.

Table 4.1: Parameters of Toyota Prius 2004

Property description	Property value	Unit
Peak phase current	250	A
Rated speed(rpm)	1200	rpm
Peak power output	50	kW
Maximum torque	400	Nm
Number of slots	48	n
Number of poles	8	n
Number of parallel branches	9	n
Yoke outer radius	134.62	mm
Yoke inner radius	116.58	mm
Stator inner radius	81.95	mm
Rotor inner radius	55.34	mm
Air gap length	0.74	mm
PM material	N362-20	-
Iron material	M19-29G	-
Winding Type	Single layer	-

The accuracy of FE modeling depends on mesh quality. The output waveforms improves with shorter time steps. However, increasing the number of mesh elements and decreasing time step size will make the computational process complicated which increase the simulation time. Hence, by experimenting with different time and space steps, an acceptable balance between simulation duration and accuracy was found when the sampling rate is set to 200 step in time and the air gap line is divided to 200 segments. To be able to calculate the flux and force density in the air gap a more condensed mesh was assigned to the stator teeth and rim, the rotor area between the magnets and the air gap. In addition, a line is placed in the middle of the air gap to calculate the force and flux density on that line. The mentioned line is segmented equal to the sampling rate which is 200. In Table.4.2, the meshing details are categorized according to the place of meshing.

Table 4.2: Meshing details

Property	Type	Max length [mm]	Max elements
Coils	Length based	2.5	1000
Magnets	Length based	3	1000
Stator rim	Length based	0.5	1000
Stator teeth	Length based	2	1000
Rotor	Length based	3	1000
Rotor2	Length based	0.5	3000
Yoke	Length based	4	1000
Property	Type	Normal deviation [deg]	Aspect ratio
Stator teeth	Surface approximation	30	5

Fig.4.1 illustrates meshing on a section of the motor surface. It can be seen that the meshing elements are more in the air gap, the rotor area between the magnets and the air gap and the stator teeth.

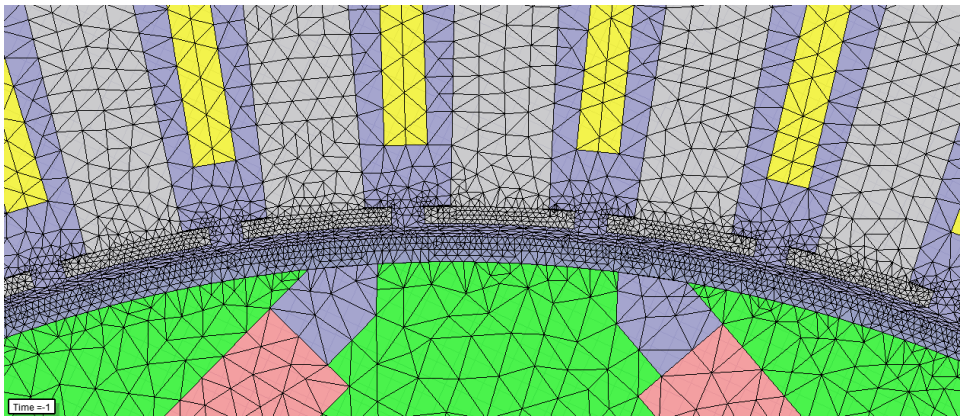

Figure 4.1: Mesh refinement in air gap

4.1 PMSM output in load operation

The excitation in FEM can be done either by voltage or current. In case of exciting the motor with voltage, the system needs longer time to reach steady state. As this study deals with several simulations and reaching steady state is time consuming, current excitation is preferred and used. Three phase sinusoidal current waveforms and their harmonic components in the frequency domain are illustrated in Fig.6.1 and Fig.4.3 respectively. Harmonic components other than the fundamental one are almost zero.

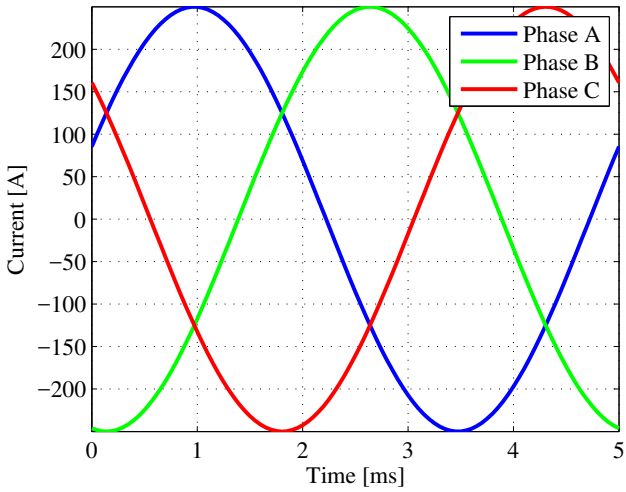

Figure 4.2: Sine phase current over one electrical period

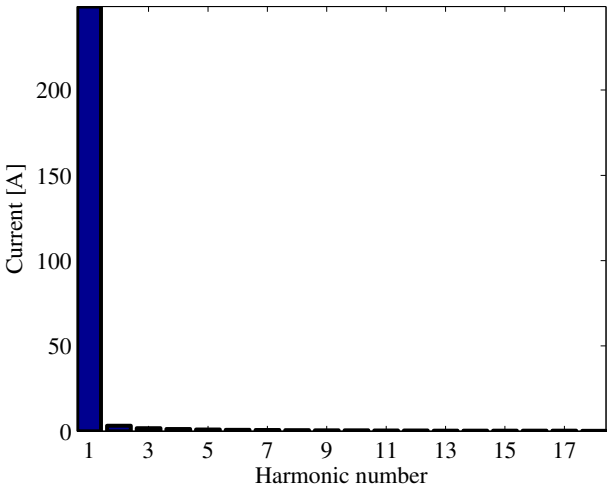

Figure 4.3: Current harmonic components

Since the current excitation is used in this simulation, distortions appear in the induced voltage. In Fig.4.4 the back EMF includes major distortions. The Fourier Transform of the back EMF presented in Fig.4.5 shows that it only contains harmonic components of odd order.

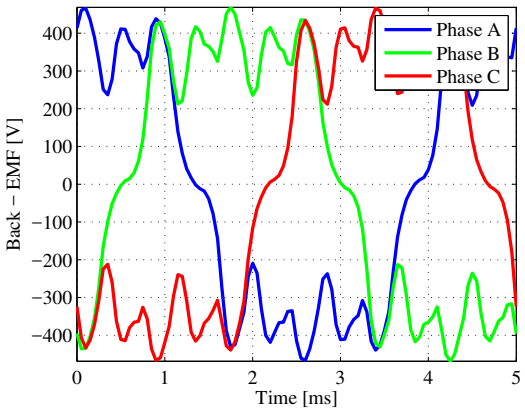

Figure 4.4: Sine phase induced voltage over one electrical period

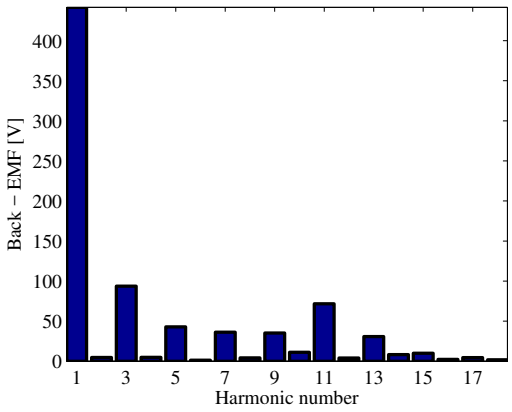

Figure 4.5: Induced voltage harmonic components

By observing Fig.4.6 the flux density distribution over rotor and stator surface in this operating point can be seen in this operating point the motor is excited with a current magnitude of 250 A and the induced voltage is 450 V. It can be seen that in the area between the magnet barriers, the stator tooth flux density is very high close to 2.4 T which means the ferromagnetic material of the rotor and stator are saturated.

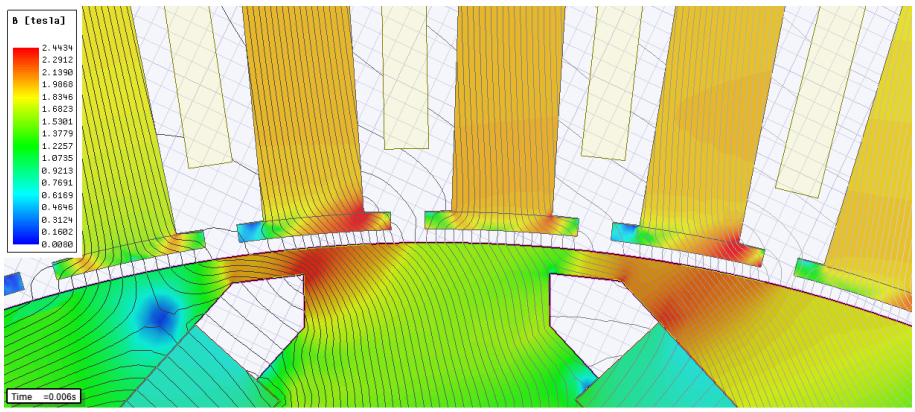

Figure 4.6

The generated electromagnetic torque of the the IPMSM in this operating point is shown in Fig.4.7 along with its harmonic components in Fig.4.8. The output torque average is equal to 246 Nm with peak to peak ripple of 52 Nm It can be seen that the torque harmonics are of the orders 6 , 12 and 18 where the 12th and 6th harmonic components are the highest. In our study the focus will be on the reduction of the harmonic components of the highest amplitude.

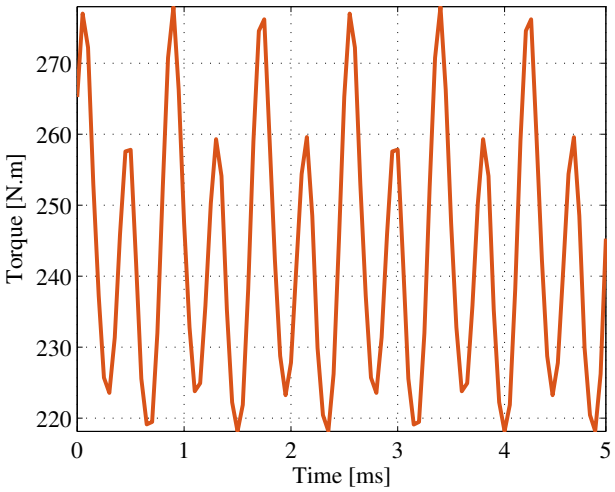

Figure 4.7: Electromagnetic torque over one electrical period

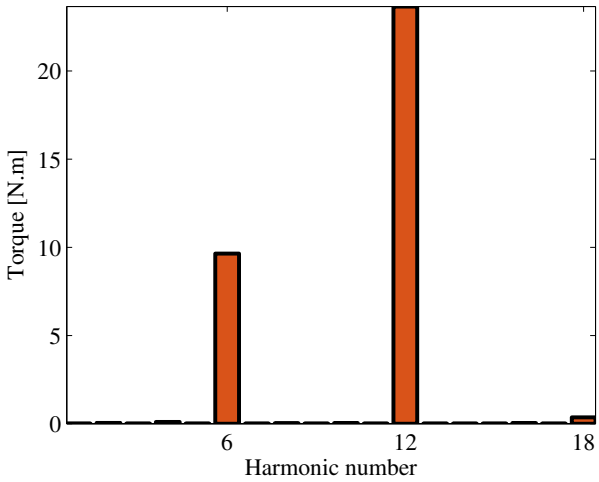

Figure 4.8: Electromagnetic torque harmonic components

4.2 Method

The method to implement the current harmonic injection and evaluate its impact on optimization of output torque is illustrated in Fig.4.9 by a flow chart. After modeling the motor according to the steps mentioned earlier, simulations are performed for 3 operating points, from different points in the torque-speed operating area of the IPMSM. In these operating points the Maximum Torque Per Ampere method which was explained in chapter 2 has been used. It is important to mention that in this study the controller is not simulated and it is assumed that the controller output is ideal and the torque reference and corresponding current reference are achieved.

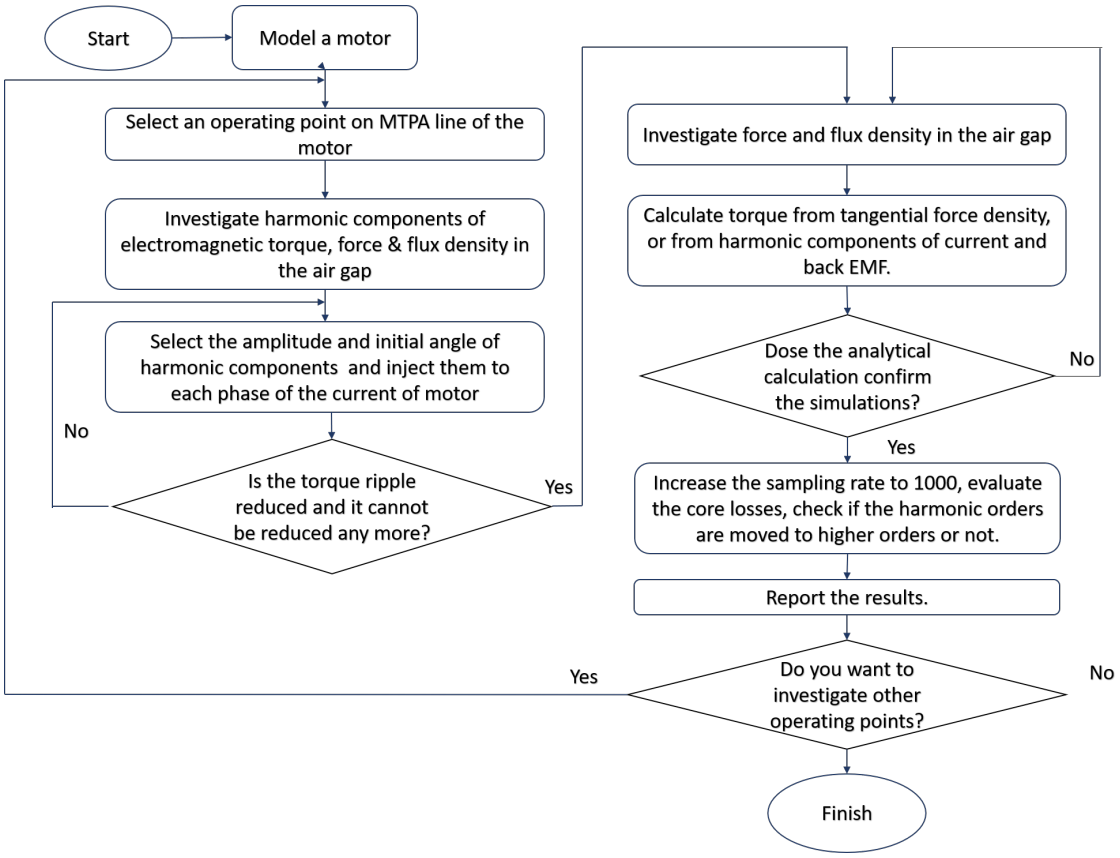

Figure 4.9: Method's flow chart for optimizing torque

In order to confirm the idea that the current harmonic injection method can cancel out the undesired effect of harmonics in the back EMF in a way that contributes to reduction of torque harmonics, various operating points at different speeds are selected. The torque ripple reduction at low speeds is more important because the torque ripple in the PMSM is a vibration source. At low speed its frequency is close to the power-train's natural frequency which might cause resonance which is one of the main reasons of the vehicle speed vibration. By reducing the torque ripple at the different speeds, the effect of the resonance can be weakened and consequently, there will be lower speed variations[5].After that, torque and back EMF harmonic need to be investigated to find the size of the harmonics that has to be injected to the current. This is done by sweeping the value of amplitude and initial phase angle of each decided harmonics. When the torque ripple reduction is the lowest possible for the corresponding operating point, the result has to be confirmed by theory and further studies on flux and force density will be done to calculate the torque analytically. Furthermore, torque can be calculated from harmonic components of current and back EMF. When the analytical results matches the simulation results, the time sampling rate should be increased to 1000 to test whether harmonics are

shifting to higher orders or not and to calculate the core losses in the stator and rotor. In chapter 6 the results for each operating point are discussed and analyzed in details based on theoretical aspects associated with the subject.

5

Electromagnetic source of torque ripple

The force distribution over stator teeth can be used to determine the torque ripple which consequently cause noise and vibration generation in a PMSM. These forces result from air gap flux density distribution, which itself is created by magnet's and armature current's field. In [17] the flux and force density's components influence on generation of NVH is closely investigated. In [18] the back EMF calculation from flux density has been studied and implemented, while in [23] electromagnetic torque calculation by Maxwell stress tensor is employed.

In the following chapter,the radial and tangential force and flux densities as well as their spatial harmonic components are closely investigated to be able to understand their impact on the back EMF and the torque in an IPMSM

5.1 Air gap flux density

The air gap flux density in a PMSM is generated by the PM in the rotor and by the armature current.

5.1.1 Rotor air gap flux density

For a PMSM, the flux density can be decomposed into its radial and tangential components

$$B = B.\hat{n} + B.\hat{t} = B_r + jB_t \tag{5.1}$$

Also, categorizing flux density with respect to its origin flux density can be defined as

$$B = B_m + B_s \tag{5.2}$$

where, B_m and B_s are flux densities in the air gap generated by the PM in the rotor and the armature current respectively. The contribution of the rotor PM in the air gap flux density by neglecting the effect of varying permeance can be expressed as

$$B_{r,m} + jB_{t,m} = \sum_{n=2k-1} B_{rm,n} \cos(np(\theta - \omega t)) + \sum_{n=2k-1} B_{tm,n} \sin(np(\theta - \omega t)) \tag{5.3}$$

where $k = 1, 2, 3, ...$, $p = P_{rotor}/P_{stator}$ is the proportion of stator pole pairs to that of the rotor, in this IPMSM it is equal to 1, ωt is the mechanical frequency and θ is the mechanical circumferential angle. Fig.5.1 and Fig.5.2 show the radial flux density in no-load operation along with its harmonic components. In order to create this condition, the stator is set to be a solid core without any slots and also the current excitation in the coils has been removed. It can be seen that B_n is a square wave which contains odd order of harmonics that confirms the above expression.

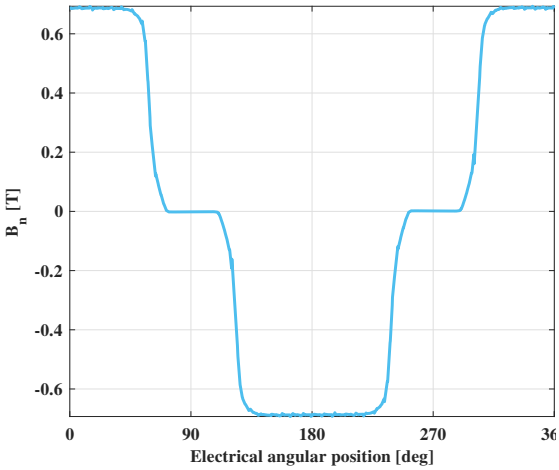

Figure 5.1: Radial flux density as a function of electrical angular position in air gap at no-load operation, solid stator

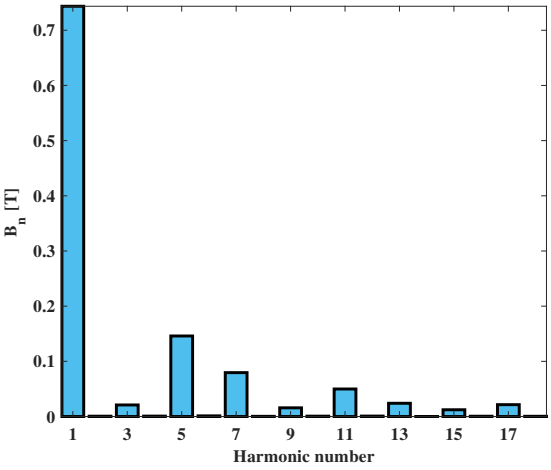

Figure 5.2: Radial flux density space harmonic components

Fig.5.3 and Fig.5.4 show B_t and its harmonic spectrum. It can be seen that B_t also contains odd order of harmonics but its value is very small and almost zero in no-load condition with a slotless stator, and they can be neglected in this case.

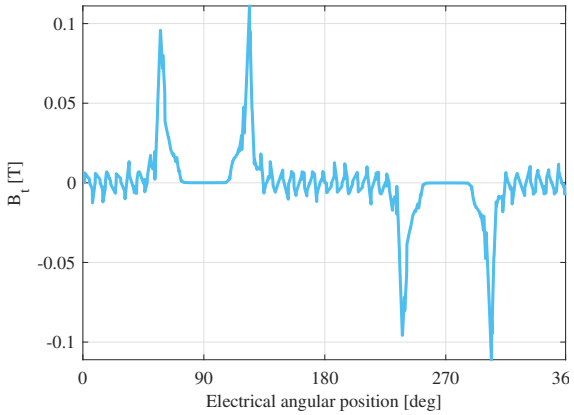

Figure 5.3: Tangential flux density as a function of electrical angular position in air gap at no-load operation, solid stator

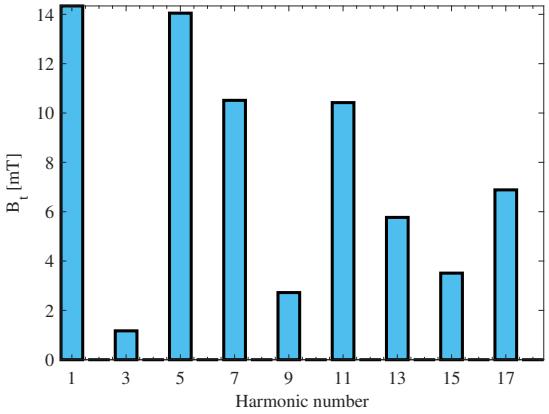

Figure 5.4: Tangential flux density space harmonic components

It is of interest to know how taking a varying permeance into account will affect flux density in the air gap. The permeance effect on flux density can be expressed in the form of Fourier series. The expression gives the permeance function in the whole air gap line, in the radial and tangential direction

$$\lambda = \lambda_a + j\lambda_b = \lambda_{g0} + \sum_{x=2k-1}^{N_\lambda} \lambda_{ax}(xN_s\theta) + \sum_{x=2k-1}^{N_\lambda} \lambda_{bx} sin(xN_s\theta) \tag{5.4}$$

where N_s is the number of slots, N_λ is the maximum order of the Fourier coefficient, x is the harmonic order and λ_{ax} corresponds to the permeance coefficient in each harmonic order in radial direction while λ_{bx} is the same coefficient defined in tangential direction. The flux density with permeance is expressed by

$$B_{slotted} = B_{slotless} \times \lambda^* \tag{5.5}$$

Therefore, the real part of the above expression is the radial flux density in the presence of a varying permeance becomes,

$$B_{rm,slotted} = B_{r,m}\lambda_a + B_{t,m}\lambda_b \tag{5.6}$$

As mentioned before, B_{tm} is close to zero so it can be neglected. Hence, B_{rm} can be rewritten as,

$$B_{r,m} \propto \sum_{u=2k-1} \sum_{x} cos(up\omega t - (up\theta \pm xN_s)) \tag{5.7}$$

Fig.5.5 and Fig.5.7 depict radial and tangential flux densities, Fig.5.6 and Fig.5.8 show the radial and tangential flux density harmonic components respectively. As

can be seen by adding the slots to the stator harmonics of order $12k \pm 1$ in which $k = 1, 2, 3, ...$, are introduced to the harmonic components in both radial and tangential direction.

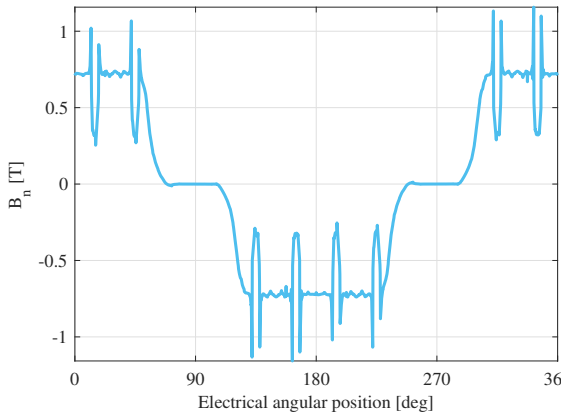

Figure 5.5: Radial flux density as a function of electrical angular position in air gap at no-load operation, slotted stator

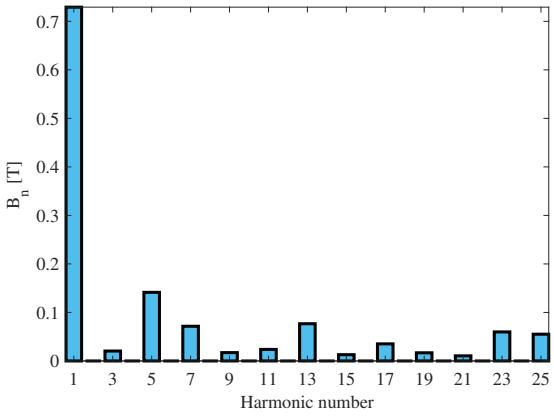

Figure 5.6: Radial flux density space harmonic components

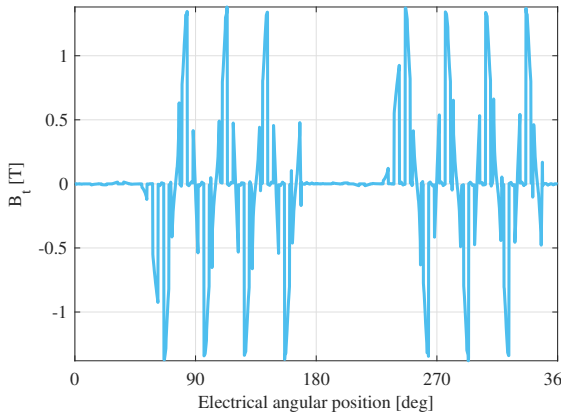

Figure 5.7: Radial flux density as a function of electrical angular position in air gap at no-load operation, slotted stator

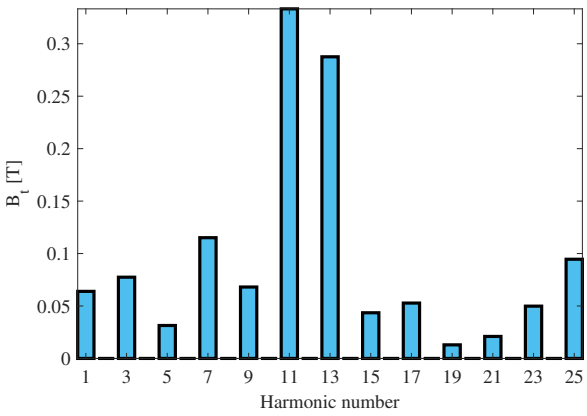

Figure 5.8: Radial flux density space harmonic components

5.1.2 Stator air gap flux density

In case of an ideal stator with even distribution of the three-phase winding, with ± 120 electrical degree shifting between phases for an alternating current, $B_{r,s}$ can

be expressed as

$$B_{r,s} \propto \cos(p\theta)\cos(\omega t) = 0.5[\cos(p\omega t - p\theta) + \cos(p\omega t + p\theta)] \tag{5.8}$$

where p is the number of pole-pair, ωt is mechanical frequency and is mechanical circumferential angle. By knowing trigonometric identity, term $\cos(p\omega t - p\theta)$ rotates backwards while $\cos(p\omega t + p\theta)$ rotates forward. According to Hopkinson's law, by exciting the armature, current flows in the stator winding, generating a flux which in turn create a magneto-motive force (MMF) in the air gap

$$B(\theta, t) = F(\theta, t)\lambda(\theta) \tag{5.9}$$

MMF waves are originating from three phase currents [17]. The harmonic components of MMF can be expressed in each phase as

$$\begin{aligned} F_{s,a} &\propto \sum_{v=2k-1} i_a cos(vp\theta) \\ F_{s,b} &\propto \sum_{v=2k-1} i_b cos(vp(\theta - \frac{2\pi}{3})) \\ F_{s,c} &\propto \sum_{v=2k-1} i_c cos(vp(\theta - \frac{4\pi}{3})) \end{aligned} \tag{5.10}$$

where i_a, i_b and i_c are the momentary phase currents at the given time instants. The amplitude of the MMF depends on the machine design such as number of turns in the stator, number of winding's layers, winding distribution factor and etc., which will be discussed later in this chapter, section 4 for calculating the back EMF. By considering the impact of the time on the MMF (4.10) can be rewritten to

$$F_{s,a} \propto \sum_{v=2k-1} cos(p)cos(vp\theta) = 0.5 \sum_{v=2k-1} [cos(p - vp\theta) + cos(p + vp\theta)] \tag{5.11}$$

$$\begin{aligned} F_{s,b} &\propto \sum_{v=2k-1} cos(p - \frac{2\pi}{3})cos(v(p\theta - \frac{2\pi}{3})) \\ &= 0.5(\sum_{v=2k-1} [cos(p - vp\theta + (v-1)\frac{2\pi}{3})] + \sum_{v=2k-1} [cos(p + vp\theta - (v+1)\frac{2\pi}{3})]) \end{aligned} \tag{5.12}$$

$$\begin{aligned} F_{s,c} &\propto \sum_{v=2k-1} cos(p - \frac{4\pi}{3})cos(v(p\theta - \frac{4\pi}{3})) \\ &= 0.5(\sum_{v=2k-1} [cos(p - vp\theta + (v-1)\frac{4\pi}{3})] + \sum_{v=2k-1} [cos(p + vp\theta - (v+1)\frac{4\pi}{3})]) \end{aligned} \tag{5.13}$$

where $k = 0, 1, 2, ...$ Therefore, the total MMF resulted from three phases can be expressed as following

$$F_s = F_{s,a} + F_{s,b} + F_{s,c} \propto \sum_{v=6k\pm1} cos(p\omega t\theta) \tag{5.14}$$

It can be seen that F_s contains harmonics of order $6k \pm 1$, whereas harmonic components of multiple 3 are shifted spatially by ± 120 electrical degrees for three phases so they do not exist in the summation of the contribution from all three phases. Therefore, radial flux density generated by the armature excitation can be expressed as

$$B_{r,s} = \Lambda F_s \propto \sum_{v=6k\pm1} cos(p\omega t\theta) \tag{5.15}$$

where the spatial harmonic component corresponding to order $v = 1, 6k - 1$ rotates forward, while $v = 6k + 1$ rotates in the backward direction. Fig.5.9 shows the air gap radial flux density. Its harmonic components can be seen in Fig.5.10 when the stator is slotless and the PM and its barriers are removed.

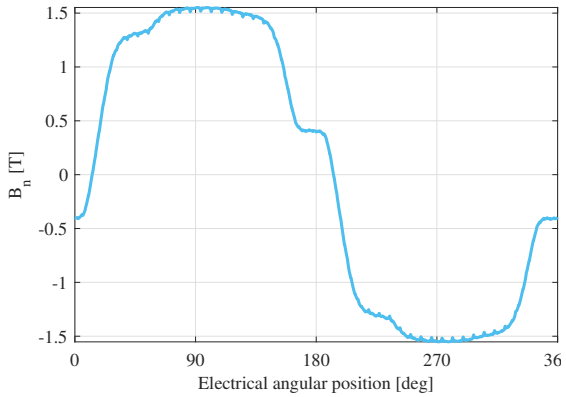

Figure 5.9: Radial flux density as a function of electrical angular position in air gap stator excitation, solid rotor and stator

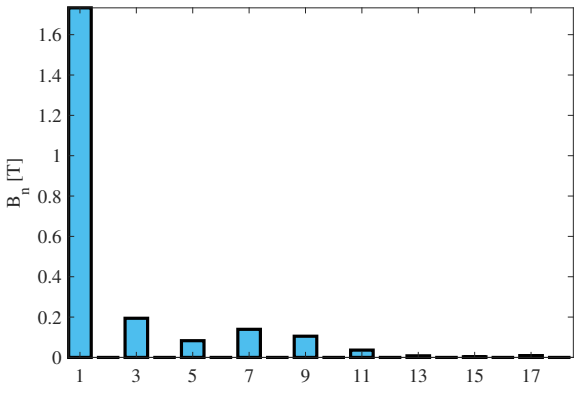

Figure 5.10: Radial flux density space harmonic components

The tangential flux density and its harmonic components can be seen in Fig.5.11 and Fig.5.12 respectively, whereas the effect of the PM and barriers in the rotor are not considered and the stator is slotless. It can be seen that under load condition B_t value is not small any more.

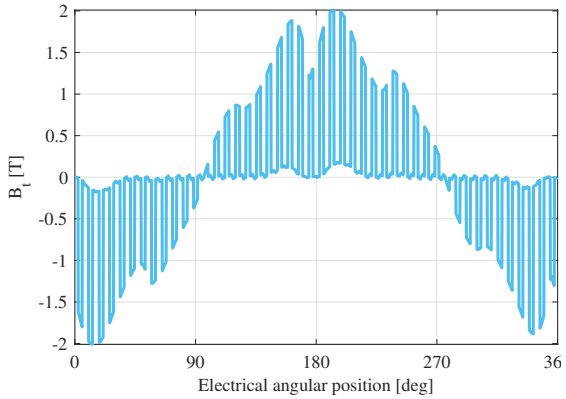

Figure 5.11: Tangential flux density as a function of electrical angular position in air gap with stator excitation, solid rotor and stator

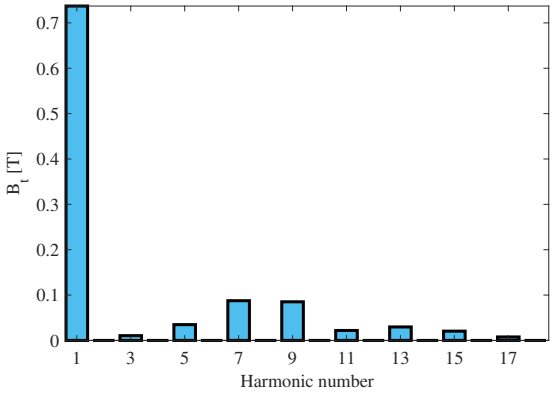

Figure 5.12: Tangential flux density space harmonic components

When making stator slotted, the permeance variation will effect the flux density waveform and the harmonic components in radial and tangential direction as observed for the no load condition. Fig.5.13 and Fig.5.15 depict the radial and tangential flux density along with their harmonic components in Fig.5.14 and Fig.5.16 respectively. As same as previous case in no load condition, the slotting of the stator increase $12k \pm 1$ orders of harmonics,when $k = 1, 2, 3, ...$

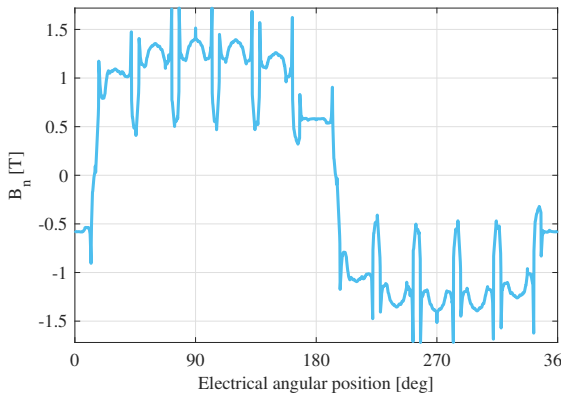

Figure 5.13: Radial flux density as a function of electrical angular position in air gap with stator excitation, solid rotor and slotted stator

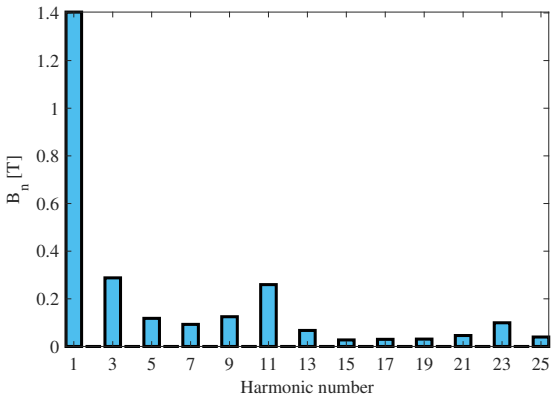

Figure 5.14: Radial flux density space harmonic components

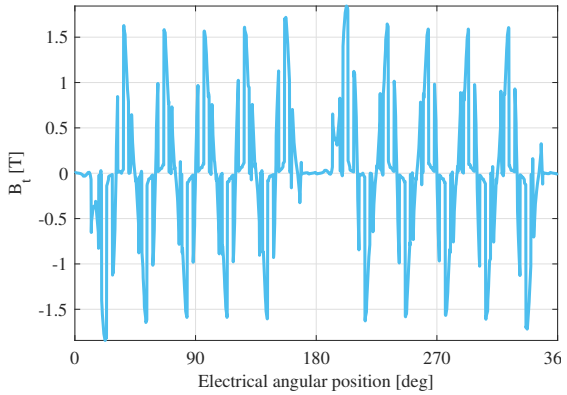

Figure 5.15: Tangential flux density as a function of electrical angular position in air gap with stator excitation, solid rotor and slotted stator

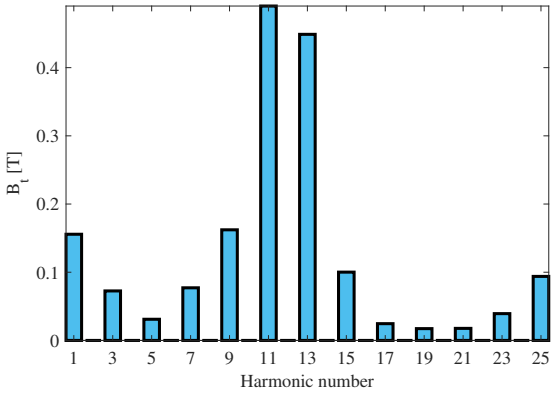

Figure 5.16: Tangential flux density space harmonic components

Finally, by substituting (4.15) in (4.9), the variable permeance is taken into account and the following expression can be obtained

$$B_{r,s} \propto \sum_{v=6k\pm1} \sum_{x} cos(p\omega t \mp vp\theta \pm xN_s) \tag{5.16}$$

In Fig.5.17 and Fig.5.19both the stator and the PMs in the rotor contribute to the generation of the flux density in the air gap, and the effect of slotting is also has been considered. The harmonic components of B_n distribution in the air gap are depicted in Fig.5.18 and Fig.5.20 showing that the flux density in the air gap only contains odd orders. Where multiples of 3 are saturation caused by magnets, and $6k \pm 1$ are caused by the non-linearity of flux, and orders corresponding to $12k \pm 1$ are increased due to slotting. Decreasing the saturation effect is out of the scope of this project The harmonic components which are of importance are the dominant ones like order of the $11, 7, 5$.

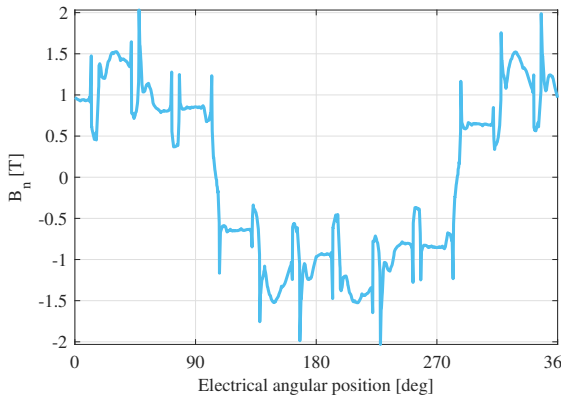

Figure 5.17: Radial flux density as a function of electrical angular position in the air gap under load, $I_{Max} = 250A$

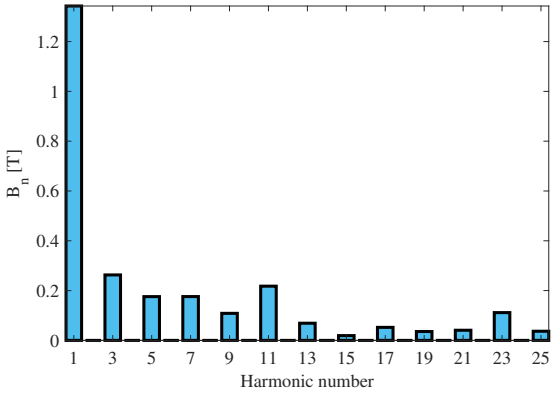

Figure 5.18: Radial flux density space harmonic components

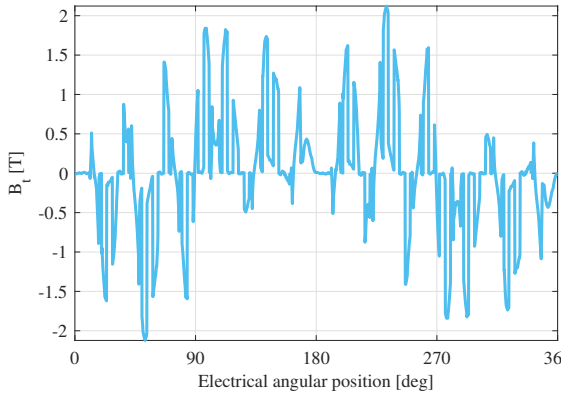

Figure 5.19: Tangential flux density as a function of electrical angular position in the air gap under load, $I_{Max} = 250A$

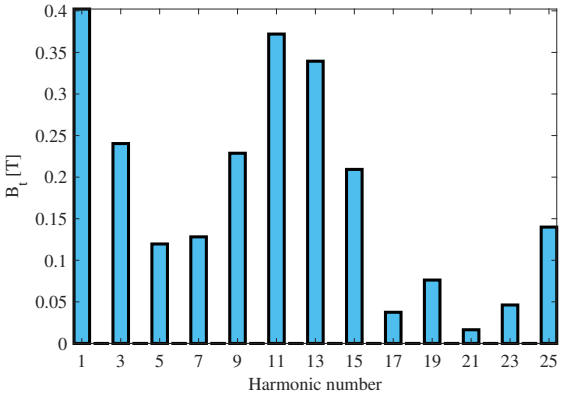

Figure 5.20: Tangential flux density space harmonic components

5.2 Air gap force density

In this section, the force density is derived according to the Maxwell stress tensor method in radial and tangential direction. The radial force is acting on the stator and is the main reason for acoustic noises and also cause vibration while the electromotive force is derived from tangential force integration on the air gap line. The derivation of torque will be discussed further in next section.

The force density in the air gap is generated by flux distribution created by the stator and rotor PM excitation and also the interaction between these two fields. In the following equation, the radial and tangential force density are derived from the

flux density in the air gap, where the effect of slotting and harmonic cross coupling is neglected for simplification.

$$f_r(,t) = \frac{1}{2\mu_0}(B_r(\theta,t)^2 - B_t(\theta,t)^2) \tag{5.17}$$

where μ_0 is the vacuum permeability equal to $4\pi \times 10^{-7} H/m$. As the B_t value in comparison with B_r is small, the force density can be considered to be

$$f_r \approx \frac{1}{2\mu_0} B_n(\theta,t)^2 = \frac{1}{2\mu_0}[B_{n,s}(\theta,t) + B_{n,m}(\theta,t)^2] \tag{5.18}$$

On the other hand, the force density is generated by the radial flux density created by the permanent magnet and stator winding. Therefore, the force density can be defined as

$$f_{r,s} \propto [\sum_v cos(p\omega t \mp vp\theta)]^2 = \sum_v cos(2p\omega t \mp 2vp\theta) \tag{5.19}$$

$$f_{r,m} \propto [\sum_u cos(up\omega t - up\theta)]^2 = \sum_u cos(2up\omega t - 2up\theta) \tag{5.20}$$

$$\begin{aligned} f_{r,sm} &\propto \sum_v \sum_u cos(p\omega t \mp vp\theta) cos(up\omega t - up\theta) \\ &= \sum_u cos(2up\omega t - 2up\theta) \\ &= \sum_v \sum_u cos[(1 \mp u)p\omega t \pm (u \mp v)p\theta] \end{aligned} \tag{5.21}$$

As can be seen from the above equations, the force density only contains even harmonics. In Fig.5.21 and Fig.5.22 the force density in the radial direction in normal operation under load is depicted along with its harmonic components.

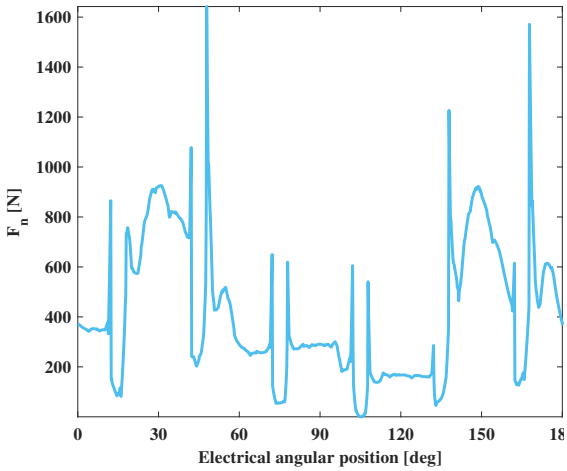

Figure 5.21: Radial force density as a function of electrical angular position in air gap under load, $I_{Max} = 250A$

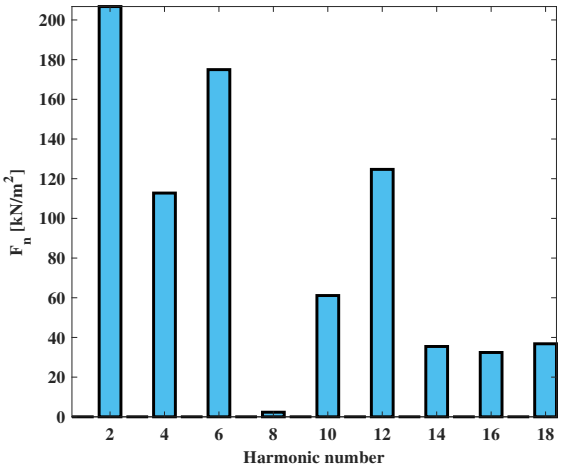

Figure 5.22: Radial force density space harmonic components

The tangential force density can be derived in the same manner, i.e from the flux density in the air gap produced by the PM using rotor and stator excitation, except the fact that B_t plays an important role to shape f_t and it has a major effect on its value and can not be neglected. The tangential force will also contain even harmonics as the radial ones.

$$f_t = \frac{1}{\mu_0}(B_r(\theta,t)B_t(\theta,t)) \tag{5.22}$$

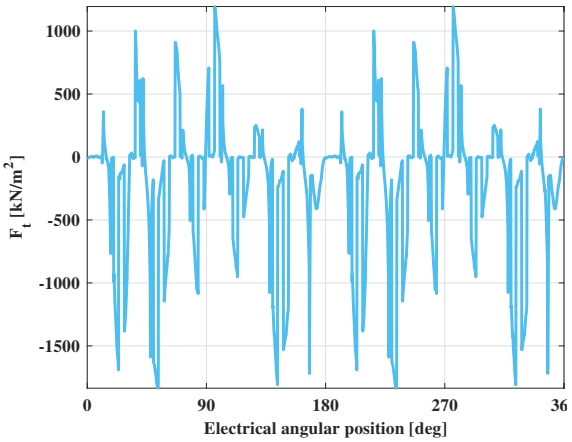

Figure 5.23: Tangential force density as a function of electrical angular position in the air gap under load, $I_{Max} = 250A$

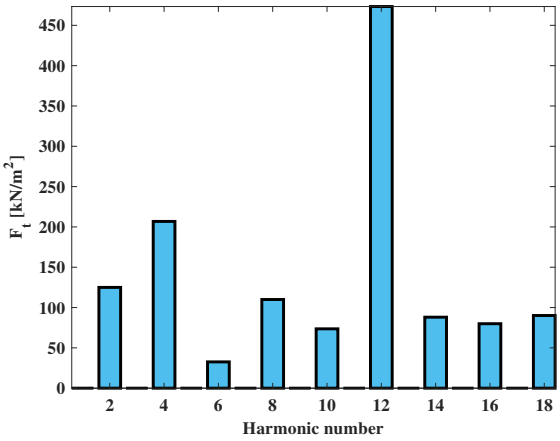

Figure 5.24: Tangential force density space harmonic components

Fig.5.23 and Fig.5.24 depict the tangential force density and its harmonic components in normal operation under load respectively. It can be seen that the amplitude of the 12th order of harmonic is significantly higher than the other orders. This can be explained by the effect of slotting of the stator which creates $12k \pm 1$ waves in the flux density and in turn $12k$ in the f_t waveform.

5.3 Electromagnetic torque calculation from air gap flux density

The electromagnetic torque is obtained from a surface integral based on the Maxwell stress tensor method on a closed surface which surrounds the rotor. In $2D$ model, the surface integral can be reduced to a line integral implemented on air gap line. As mentioned in (5.2) the electromotive force in the tangential direction can be derived from the flux density in the radial and tangential direction over the introduced air

gap line expressed as

$$T_{em} = \frac{1}{\mu_0} \int_0^{2\pi} r^2 B_r B_\theta d\theta = \int_0^{2\pi} r^2 f_t d\theta \tag{5.23}$$

where $r = 80.575$ mm is the air gap line radius in the middle of the inner stator and outer rotor radii. In other words, the torque is created by tangential force acting along the air gap path. This method can be independent of the radius in an approximate solution. The electromagnetic torque is a resultant from the integration of the tangential force over the whole air gap line. Therefore, when calculating torque in a sector including only one pole pair, the torque equation in discrete solution can be rewritten as

$$T_{em} = \frac{PL_e}{\mu_0} \sum_{i=1}^{N_A} r^2 B_{ri} B_{\theta i} \theta_i = \frac{PL_e}{\mu_0} \sum_{i=1}^{N_A} r^2 f_{ti} \theta_i \tag{5.24}$$

where P is the number of pole pairs, $L_e = 83.82mm$ is the effective length of the motor, and N_A is the number of the total time instants that the summation is conducted on. The analytically calculated electromagnetic torque from above the expression in the MATLAB and result from FE analysis are illustrated in Fig.5.25 along with its harmonics in Fig.5.26. It can be seen that the dominating harmonic components in the torque from the Maxwell are of order of multiple six while the 12th order is by far the highest, while the analytically calculated torque also consist of other even harmonics. By comparing the results from the simulation and calculation, approximately 35% variation can be seen due to inaccuracy in the solution and meshing in the simulation, but this calculation can be used for future comparison as the solution will remain the same. Hence, in chapter 6 by comparing the results from analytically calculated torque before and after the current harmonic injection by considering the calculation error, would be a valid comparison.

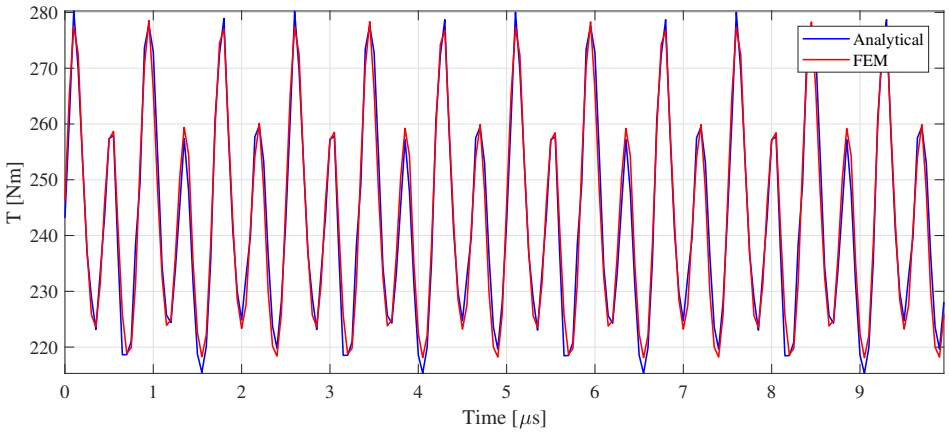

Figure 5.25: Electromagnetic torque under load operation, $I_{Max} = 250$ A

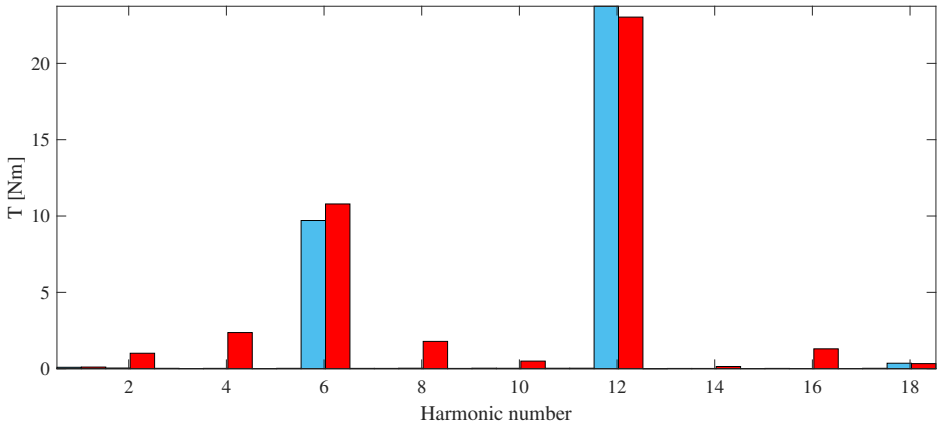

Figure 5.26: Electromagnetic torque time harmonic components

6

Theoretical analysis of the results

In this section, the effect of the current harmonic injection method on the undesired harmonics of the the back EMF and the torque is investigated. As was mentioned previously, in this study the machine is excited with pure sinusoidal armature currents, but the generated back EMF waveforms contains different harmonic components which cause torque pulsations. In order to reduce the undesired torque harmonics, the current harmonic injection method is used. In the presented method, first the highest back EMF harmonics are determined, then the same current harmonics order are injected into the armature currents in each phase to cancel out the negative effect of the back-EMF harmonics on the torque ripple. After that, the optimal amplitudes and phase angles of the current harmonics are determined by sweeping. It is important to know that in each operating point, the harmonic components of the back EMF vary and the current harmonic injection can be a combination of different orders. As discussed in chapter 3 the current harmonic components can be injected to each phase by the following equations

$$\begin{aligned} I_a &= I_1 sin(\omega t + \theta) + I_5 sin(-5\omega t + \beta_5) \\ &\quad + I_{11} sin(-11\omega t + \beta_{11}) + I_{13} sin(13\omega t + \beta_{13}) \end{aligned} \tag{6.1}$$

$$\begin{aligned} I_b &= I_1 sin(\omega t + \theta - \frac{2\pi}{3}) + I_5 sin(-5(\omega t - \frac{2\pi}{3}) + \beta_5) \\ &\quad + I_{11} sin(-11(\omega t - \frac{2\pi}{3}) + \beta_{11}) + I_{13} sin(13(\omega t - \frac{2\pi}{3}) + \beta_{13}) \end{aligned} \tag{6.2}$$

$$\begin{aligned} I_c =& I_1 sin(\omega t + \theta + \frac{2\pi}{3}) + I_5 sin(-5(\omega t + \frac{2\pi}{3}) + \beta_5) \\ &\quad + I_{11} sin(-11(\omega t + \frac{2\pi}{3}) + \beta_{11}) + I_{13} sin(13(\omega t + \frac{2\pi}{3}) + \beta_{13}) \end{aligned} \tag{6.3}$$

where β_n is the initial angle of the current harmonic. The amplitude of the initial phase of the current harmonic components in each phase is obtained from sweeping to reduce the torque ripple to an accepted value. For each operating point, the addition of each harmonic component is studied individually and the most suitable combination with the lowest torque ripple is chosen. In the following, 3 operating

points have been studied and the result will be discussed and analyzed with respect to the torque calculation as discussed in chapter 3 and also by looking at the field distribution in each case before and after injection to see the changes.

6.1 First operating point results

First, operating point specification is classified in Table.6.1. The results for this operating point are classified in 5 different cases. The first case is the normal operation when no injection has been done, second, third and forth case correspond to separately injecting the 5th, 11th and 13th current harmonic respectively. The fifth case is a combination of all three harmonic component in single injection.

Table 6.1: First operating point specifications

Current peak [A]	Voltage peak [v]	Average torque [Nm]	Speed [RPM]
250	441	247	3000

In the normal operation without any injection, the waveforms of the input current in the three phases are purely sinusoidal so the harmonic components, except the fundamental one are zero, but by intentionally adding harmonics to the current, its waveforms become non-sinusoidal and the harmonic components are changed. The injection has been done in such a way that the three phase currents remain symmetrical and the orders of current harmonic are chosen based on the one in voltage that are the highest. In this operating point, the considerable ones from the highest amplitude to the lowest are harmonic orders of $11, 13, 5, 7$. Fig.6.1 and Fig.6.2 depict the current waveforms and the harmonic spectrum in the defined 5 cases respectively. As can be seen, the currents in each case only contain the harmonic components that intentionally have been added to it. In this operating point, the addition of the 7th and 5th harmonic have the same effect, so only the impact of the 5th harmonic is presented, and later used to decrease the torque ripple in the output.

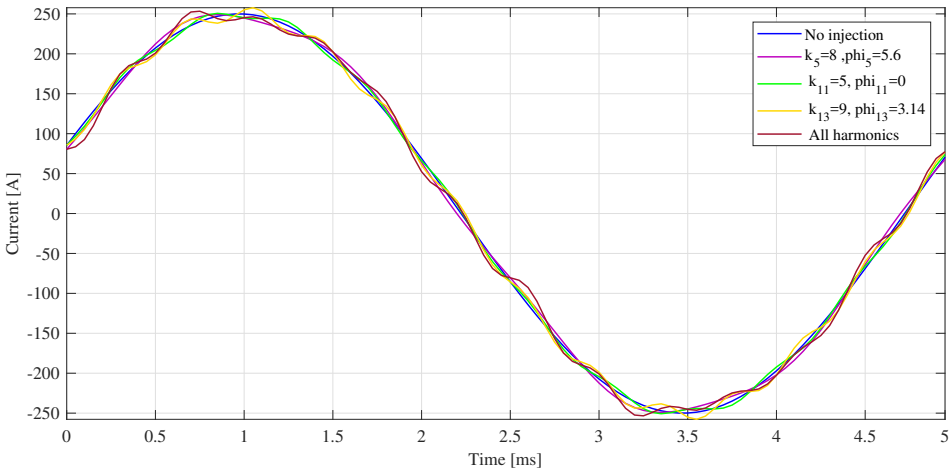

Figure 6.1: Phase input current of IPMSM with different current harmonic injection

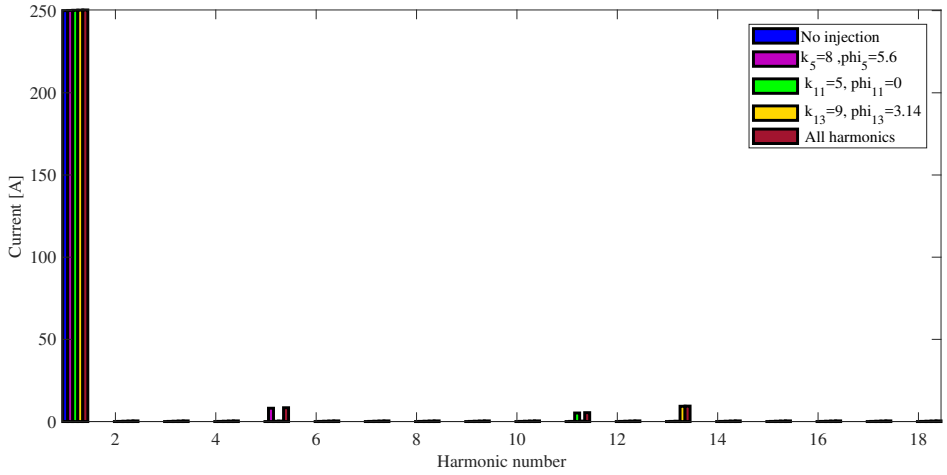

Figure 6.2: Phase input current harmonic components of IPMSM with different current harmonic injections

Table.6.2 shows the final Fourier coefficient and initial angle of each current harmonic component obtained after parameter sweeping, which results in the most desirable impact on the torque ripple.

Table 6.2: Values of current harmonics with and without injection

Injection	5th	11th	13th
Without injection	0	0	0
Injection of I_5	$8e^{j1.78\pi}$	0	0
Injection of I_{11}	0	5	0
Injection of I_{13}	0	0	$9e^{j\pi}$
Injection of $I_5 + I_{11} + I_{13}$	$8e^{j1.78\pi}$	5	$9e^{j\pi}$

The magnitude of the back EMF harmonics for different cases is illustrated in Table.6.3. Fig.6.3 and Fig.6.4 show the output torque and its harmonic in different

Table 6.3: Value of the Back EMF harmonics with and without injection

Injection	5th	7th	11th	13th	17th	23th
Without injection	41.12	37.52	69.58	35.77	2.9	10.29
Only injection of I_5	25	21.55	70	34.6	7.35	12.93
Only injection of I_{11}	39.24	35.12	69.4	35.4	6.39	8.32
Only injection of I_{13}	38.3	33.3	75.9	71.5	10.16	12.94
Injection of $I_5 + I_{11} + I_{13}$	23.42	18.18	95.19	94.44	17.8	17.76

cases respectively. As can be seen, the most desirable result is obtained from injection of all harmonic orders of $5th, 11th, 13th$ together, which is depicted in red color in the figures.

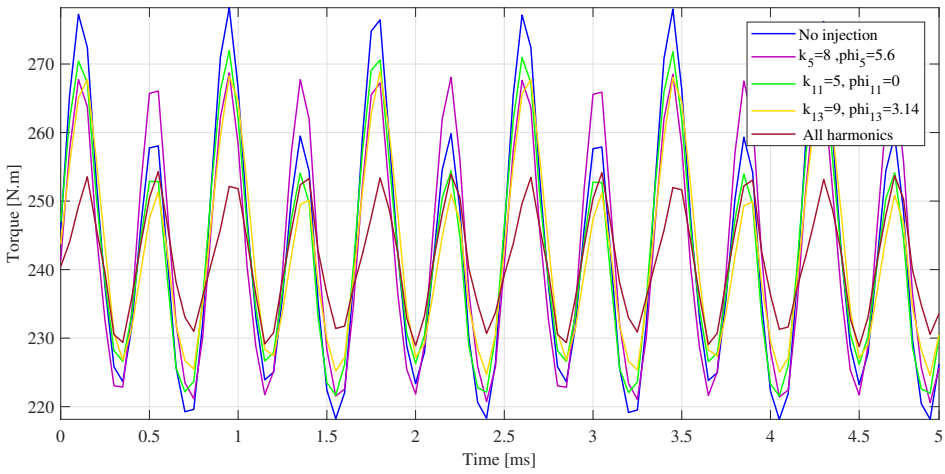

Figure 6.3: Electromagnetic torque of IPMSM with different current harmonic injection

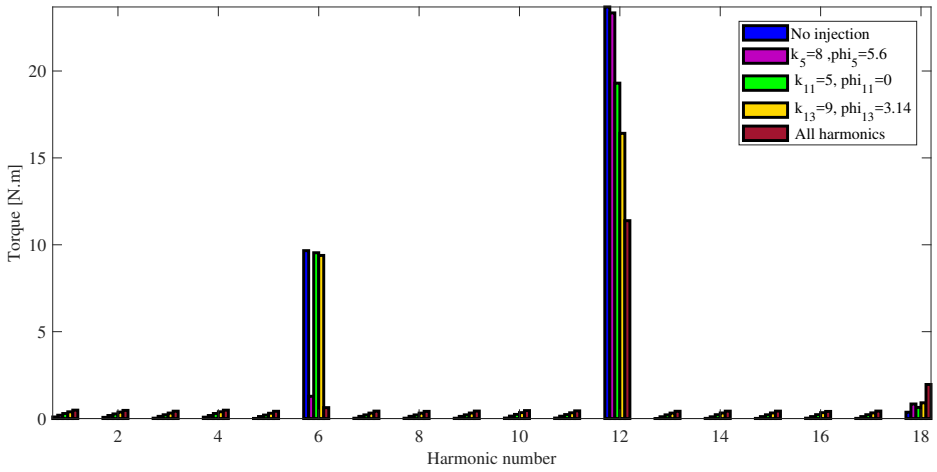

Figure 6.4: Electromagnetic torque harmonic components of IPMSM with different current harmonic injections

As shown in Fig.6.4 and Table.6.4 the 5th harmonic injection has the highest impact on the 6th harmonic component while the 11th and 13th harmonic reduces the 12th harmonic component of the torque. So to be able to reduce the whole ripple in the torque, both the 6th and 12th harmonic should be reduced to the lowest possible value. Therefore, the combination of these three harmonic components can reduce the 6th order harmonic of the torque to 0.2 Nm and the 12th one to 10.98 Nm which is approximately equal to half of its original value of 23.66 Nm.

Table 6.4: Magnitude of the toque harmonics with and without injection

Injection	6th	12th
Without injection	9.61	23.66
Injection of I_5	1.16	23.11
Injection of I_{11}	9.29	19.12
Injection of I_{13}	9.16	16.15
Injection of $I_5 + I_{11} + I_{13}$	0.2	10.98

In Fig.6.5 the torque ripple in different cases are depicted. The torque ripple is expressed as

$$T_{ripple} = \frac{T_{Max} - T_{Min}}{T_{Avg}} \times 100 \tag{6.4}$$

In case of no current harmonic injection and normal operation, the torque ripple is equal to 25% which reduces to almost 20% when the 5th harmonic is injected. In case 3 when the 11th harmonic component is added to the main current the torque ripple becomes 21% and in case 4 by injecting the 13th harmonic component which has the highest back EMF harmonic component amplitude, the torque ripple is close to 19%. These values show that the 13th harmonic individually has the highest impact on the torque ripple while the 11th harmonic has the least effect. Hence, the summation of all these contributions result in a 14% reduction in torque ripple.

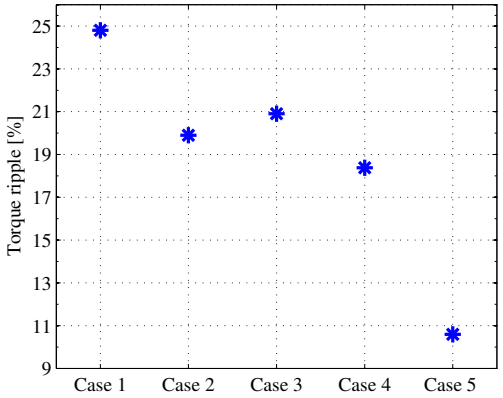

Figure 6.5: Torque ripple percentage in different cases of injecting current harmonic

6.2 Second operating point results

To be able to validate the current harmonic injection method, 2 other operating points are investigated. The second operating point specification is classified in Table.6.5. In this operating point, the chosen values of Fourier coefficients after experimenting with different harmonic injections are classified in 4 different cases. The first case is the normal operation when no injection has been done, second, third case correspond to separately injecting the 7th, 11th harmonics respectively. The fourth case is injection of both harmonic components together.

Table 6.5: Second operating point specifications

Current peak [A]	Voltage peak [V]	Average torque [Nm]	Speed [RPM]
77.33	222.17	104.11	2106

This operating point is one of the most commonly used operating points in this machine with a speed of 2106 RPM, an RMS current value of 54.7 A with current angle of 39 degrees was found to be appropriate(values were obtained from the data sheet of the machine). The average torque at this operating point is 104.11 Nm with a torque ripple of 29%. In order to reduce the torque ripple, the same method is used and the different parameters of current harmonics are determined and added to the input currents. The current harmonic components values injected in each case are illustrated in Table.6.6.

Table 6.6: Value of current harmonics with and without injection

Injection	7th	11th
Without injection	0	0
Injection of I_7	$3.5e^{j1.21\pi}$	0
Injection of I_{11}	0	$8e^{j1.53\pi}$
Injection of $I_7 + I_{11}$	$3.5e^{j1.21\pi}$	$8e^{j1.53\pi}$

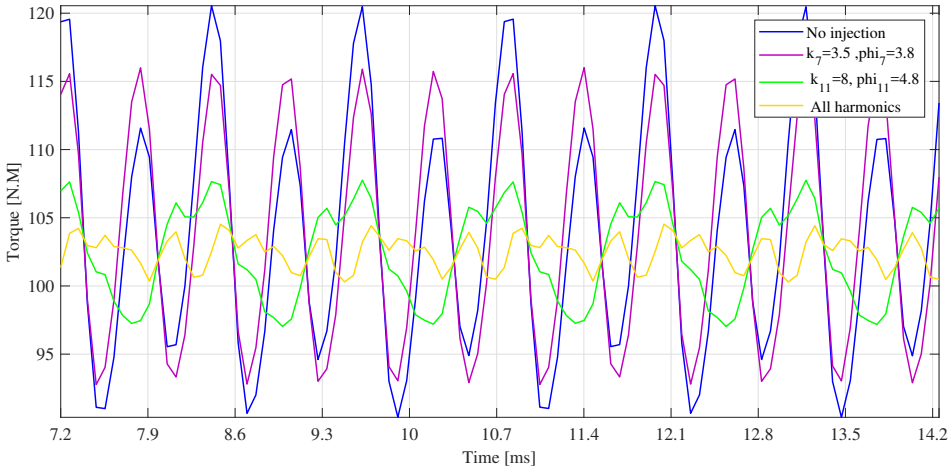

Figure 6.6: Electromagnetic torque of the IPMSM with different current harmonic injections

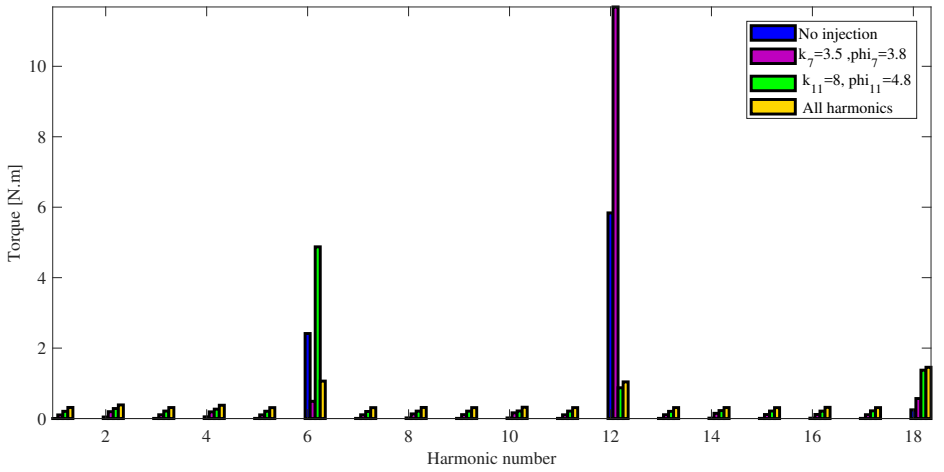

Figure 6.7: Electromagnetic torque harmonic components of the IPMSM with different current harmonic injections

Table 6.7: Magnitude of the torque harmonics with and without injections

Injection	6th	12th
Without injection	2.41	5.84
Injection of I_7	0.5	11.68
Injection of I_{11}	4.88	0.88
Injection of $I_7 + I_{11}$	1.06	1.05

After current injection, the torque ripple has a significant reduction and it is decreased to 4.22%, In table 6.7 the reduction of undesired torque harmonics are

shown for different injections, In the last case, which is the injection of the 7th and 11th current harmonics together, the harmonics of the torque are almost close to 1 which is very small compared with normal case without injection.

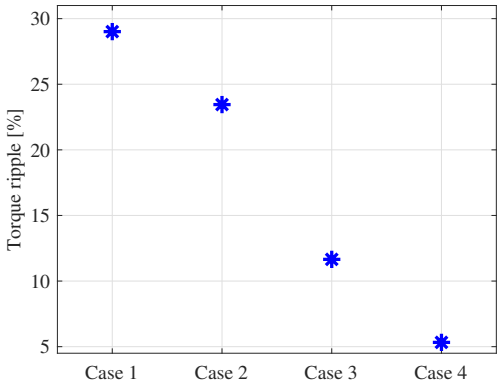

Figure 6.8: Torque ripple percentage in different cases of injecting current harmonic

6.3 Third operating point results

The specifications for the third operating point is presented in Table.6.8. In this operating point after running simulations and sweeping the Fourier coefficients, the 5th and 11th harmonic components injection has the best impact on torque ripple reduction. The simulation has been done in 4 steps. The first case is the normal operation when no injection has been done, second, third case correspond to separately injecting the 5th, 11th harmonic components respectively. The fourth case is injection of both harmonic components together to the armature currents. All cases are classified in Table.6.9

Table 6.8: Third operating point specifications

Current peak [A]	Voltage peak [V]	Average torque [N.m]	Speed [RPM]
110.73	110	159.4	905

The torque ripple in this operating point without any compensation is equal to 27%, its waveforms is shown in blue color in Fig.6.9 along with its harmonic components in Fig.6.10. As illustrated in Table.6.10, the first row shows that the 6th and 12th magnitude of the harmonic components are equal to 3.68 and 16.58 Nm respectively which are reduced to 0.36 and 0.83 Nm after injecting the 5th and

Table 6.9: Value of current harmonics with and without injection

Injection	5th	11th
Without injection	0	0
Injection of I_5	$2e^{j1.2\pi}$	0
Injection of I_{11}	0	$11e^{j.59pi}$
Injection of $I_5 + I_{11}$	$2e^{j1.2\pi}$	$11e^{j.59pi}$

11th harmonics at the same time to the current. The resultant torque has a low torque ripple, approximately equal to 7%.

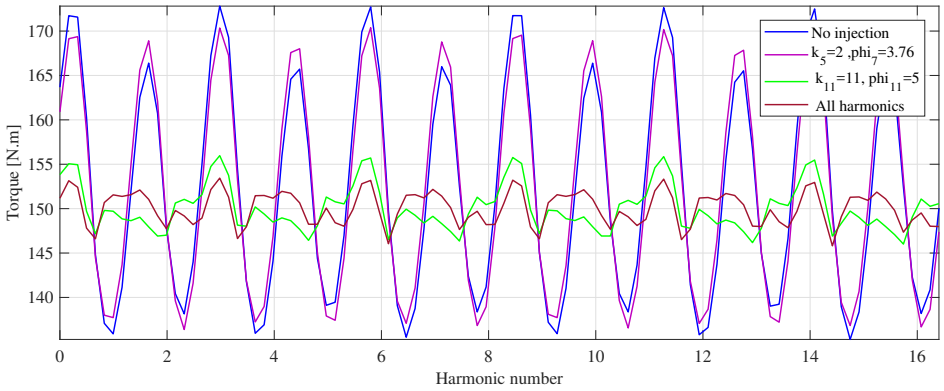

Figure 6.9: Electromagnetic torque of the IPMSM with different current harmonic injections

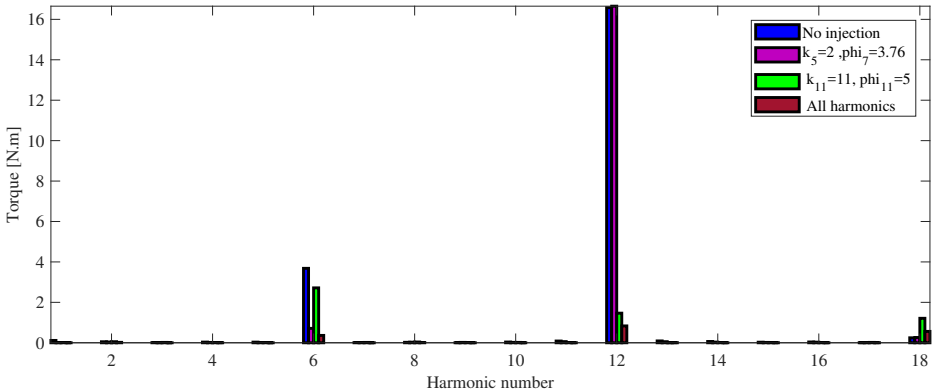

Figure 6.10: Electromagnetic torque harmonic components of the IPMSM with different current harmonic injections

The torque ripple variation obtained from the compensation of current is illustrated in Fig.6.11, while the exact amplitude of the $6th$ and $12th$ harmonics for all four cases as defined before, can be seen in Table 6.10.

Table 6.10: Magnitude of the toque harmonics with and without injection

Injection	6th	12th
Without injection	3.68	16.58
Injection of I_5	0.71	16.65
Injection of I_{11}	2.72	1.47
Injection of $I_5 + I_{11}$	0.36	0.83

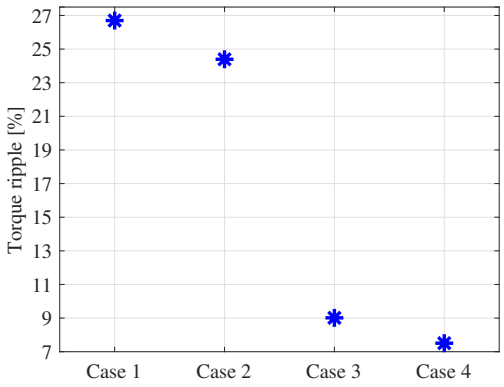

Figure 6.11: Torque ripple percentage in different cases of injecting current harmonic

6.4 Analysis of results

6.4.1 Back EMF and current investigation

According to the torque equations explained previously in chapter 4, the electromagnetic torque can be calculated from the summation of the average torque and its harmonic components expressed as

$$T_{em} = T_1 + T_2 + T_3 + T_4 \tag{6.5}$$

$$T_1 = \frac{3E_1 I_1}{2\omega} \cos(\theta) \tag{6.6}$$

$$T_2 = \frac{3E_v I_1}{2\omega} \sum_v \cos\left[(k_{ev} v - 1)\,\omega t + \theta - \alpha_v\right] \tag{6.7}$$

$$T_3 = \frac{3E_1 I_u}{2\omega} \sum_u \cos\left[(1 - k_{iu} u)\,\omega t + \beta_u\right] \tag{6.8}$$

$$T_4 = \frac{3E_v I_u}{2\omega} \sum_v \sum_u \cos\left[(k_{ev} v - k_{iu} u)\,\omega t + \beta_u - \alpha_v\right] \tag{6.9}$$

where T_1 is the average torque and T_2 is torque ripple, caused by the fundamental value of current and the harmonics of the back EMF, T_3 is torque ripple caused by the fundamental value of the back EMF and the current harmonics, T_4 can be either a constant value or a sinusoidal signal depending on the order of the current and back EMF harmonics.
In order to validate the results from the simulations, the output torque for the first operating point is calculated analytically with the mentioned equations and compared with the simulation result. Then the effect of the 5th order harmonic is added and the comparison between simulation and analytic calculation is done. In case of normal operation without any current harmonic injection, as was discussed earlier, although there are pure sinusoidal input currents, the generated back EMF contains odd harmonic orders. Therefore, only T_1 and T_2 exist. T_2 depends on the current fundamental component, magnitude and initial angle of different harmonic components of the back EMF. The first step done to conduct this analysis is to do the Fast Fourier Transform (FFT) on current and back EMF obtained from a simulation using Maxwell. Then T_2 is generated by MATLAB from harmonic components until order 20 which is the highest one. The sinusoidal waveforms of each torque harmonic component explained as T_2 are depicted in Fig.6.12.

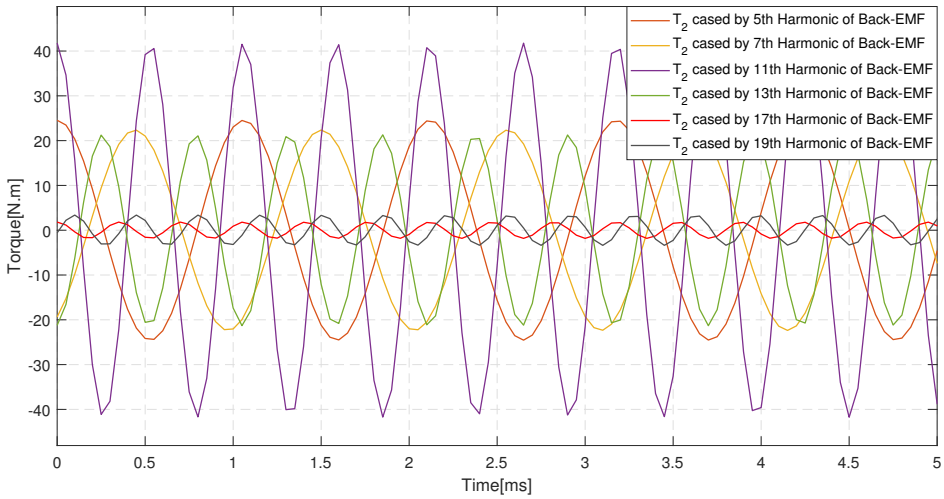

Figure 6.12: Torque Harmonic waveforms generated by the fundamental current component and the back EMF harmonic components

By adding all the T_2 waveforms from different harmonic orders to the average torque which is 247 Nm the output torque is obtained as presented in the Fig.6.13. The resulting torque from this method is an approximate calculation to prove the simulations are following the theory. In order to have an exact waveform of the

output torque, all the back EMF harmonics must be considered.

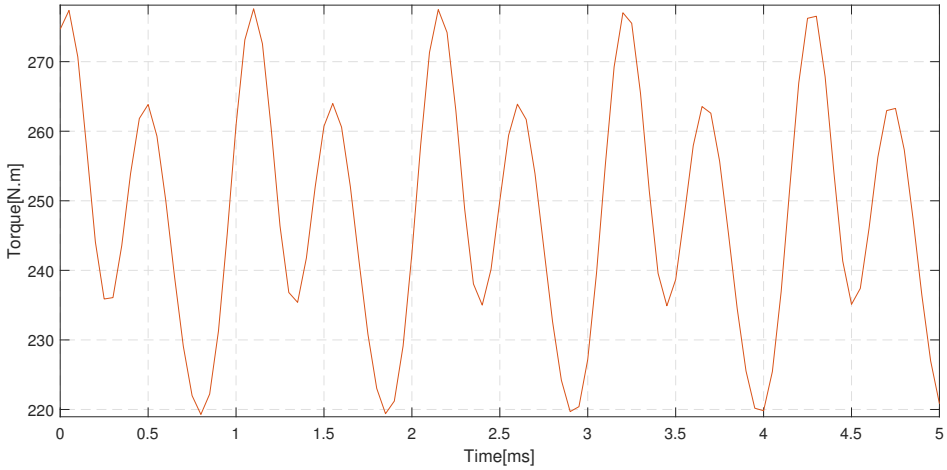

Figure 6.13: The output torque harmonics calculated analytically from T_1 and T_2 elements

In order to realize the effect of the current harmonic injection, the same procedure is implemented to create the output torque after current harmonic injection. In this case, in addition to T_2 coming from the back EMF harmonics, the T_3 waveforms appear due to the injected current harmonics to the current waveform. For the sake of simplicity, only the impact of the $5th$ order of current harmonic is investigated. Fig.6.14 shows the T_2 and T_3 waveforms in different harmonic orders.

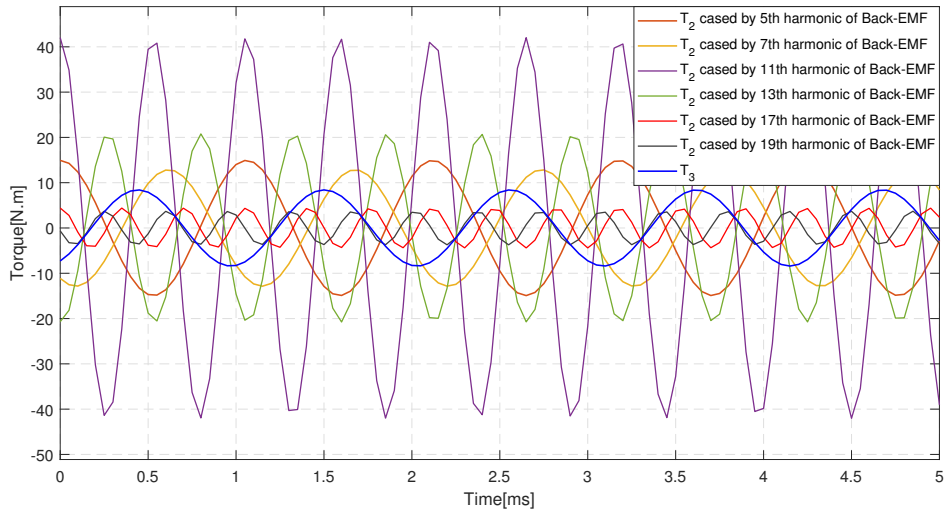

Figure 6.14: The output torque harmonics calculated analytically from T_1 and T_2 elements after injection I_5

Finally, by adding all T_2 curves, T_3 and the average torque, the output torque is created as shown in Fig.6.15. By comparing the torque before and after injection it can be seen that the torque ripple is decreased and it confirms the simulation results. The difference in torque content before and after injection is clearly caused by the addition of T_3 and also the magnitude reduction in the T_2 elements, which consequently reduces the torque ripple from 25% to 20%.

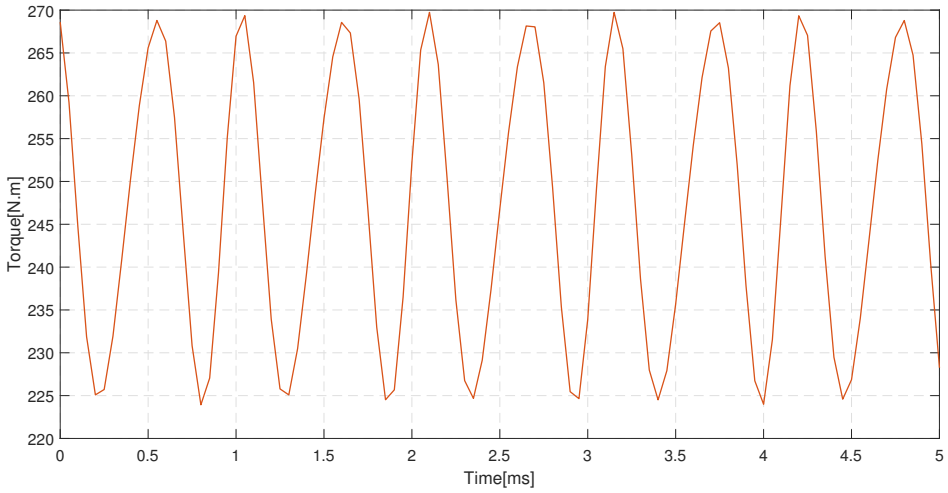

Figure 6.15: The output torque calculated analytically from T_1 and T_2 and T_3 elements after $5th$ current injection

6.4.2 Flux and force density investigation

Another approach to investigate the results obtained from the current injection method is to analyze the changes in flux and force density harmonic contents. As discussed in chapter 5 the electromagnetic torque is generated by the tangential force acting on the rotor and the tangential force itself is created by the flux density in the radial and tangential direction. The equations explaining the relation between the torque, force and flux density is expressed as

$$T_{em} = \frac{1}{\mu_0} \int_0^{2\pi} r^2 B_r B_\theta d\theta = \int_0^{2\pi} r^2 f_t d\theta \tag{6.10}$$

To be able to see the impact of the implemented torque optimization method on the field content, the second operating point's flux and force density have been investigated and the results are presented in the following. The flux generated in the air gap, is not only a varying value as a function of space, but it also changes as the rotor moves in time. Hence, investigating the flux and force density harmonic contents in a single position or a single time instant, is not sufficient to interpret the

current injection method effect on the field contents. Fig.6.16 and Fig.6.17 depict B_n waveform and component as a function of time for a single point of the air gap line and its harmonic components respectively. In this single position in some cases the harmonic components of the B_n are decreased or remain constant while some has been increased but it is not possible to draw a conclusion from this changes. By taking into account the space harmonics of B_n for a time instant, as shown in Fig.6.19, it can be seen that space harmonic simultaneously is facing reduction in some orders.

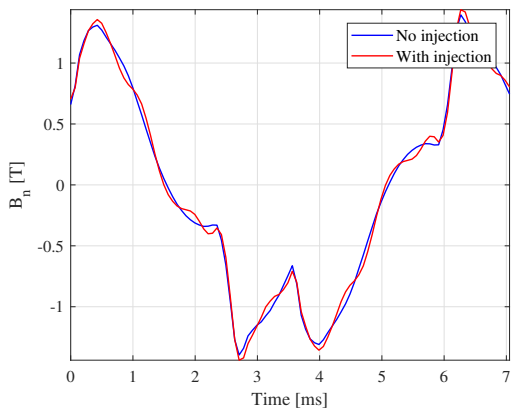

Figure 6.16: Radial flux density as a function of time before and after current harmonic injection

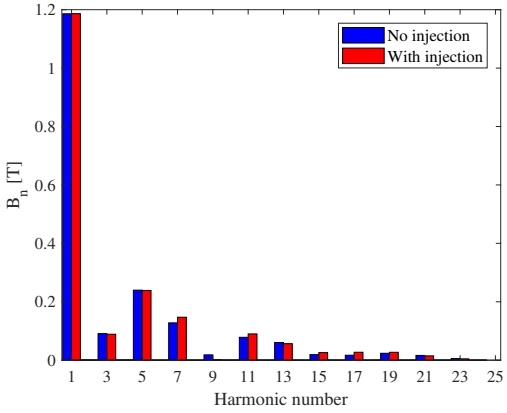

Figure 6.17: Radial flux density time domain harmonic component before and after current harmonic injection

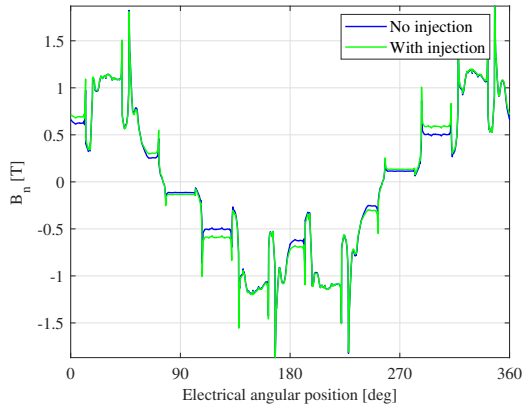

Figure 6.18: Radial flux density as a function of electrical angular position before and after current harmonic injection

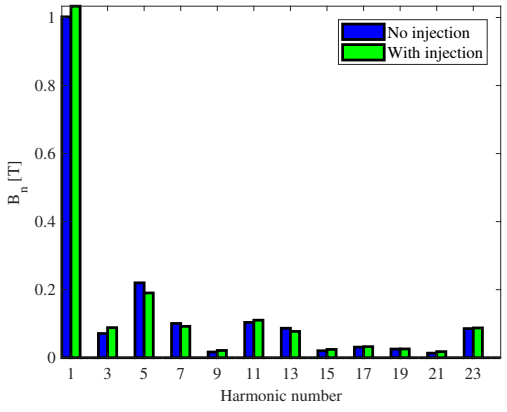

Figure 6.19: Radial flux density space domain harmonic component before and after current harmonic injection

As mentioned before, the tangential force density is created by multiplication of

the radial and tangential flux density. So, to be able to analyse the force density harmonic contents, the tangential flux density contents should be investigated in the same way. It can be seen in the time harmonic spectrum of B_t in Fig.6.21 and its space harmonics in Fig.6.23that B_t is also reduced in some cases. The final effect of this changes resulting in the force density in time and space domain can be seen in Fig.6.25 and Fig.6.27 respectively.

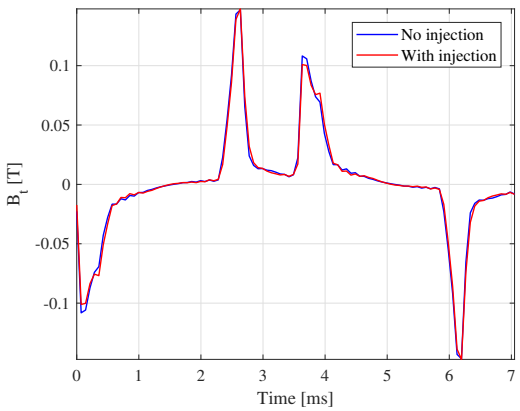

Figure 6.20: Tangential flux density as a function of time before and after current harmonic injection

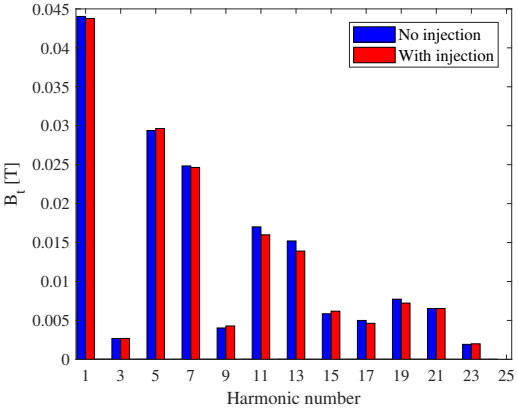

Figure 6.21: Tangential flux density time domain harmonic component before and after current harmonic injection

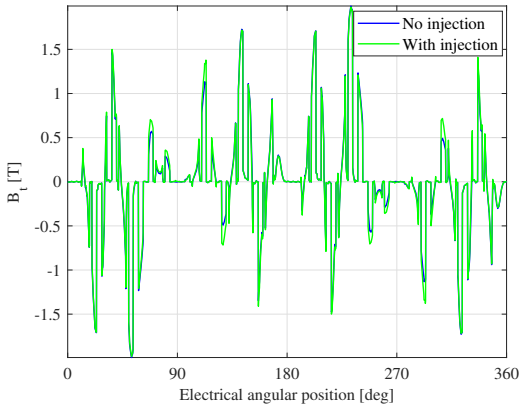

Figure 6.22: Tangential flux density as a function of electrical angular position before and after current harmonic injection

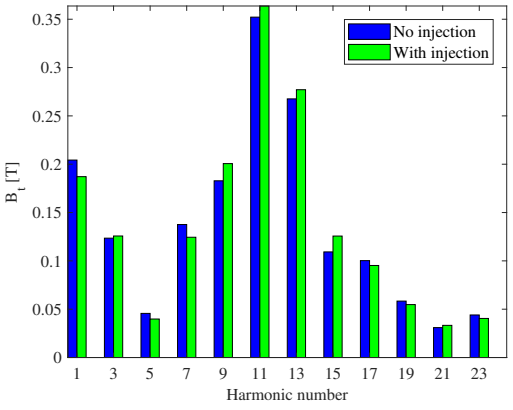

Figure 6.23: Tangential flux density space domain harmonic component before and after current harmonic injection

It is fair to say, that the force density harmonics in space are mostly decreased for the selected time instant but the time harmonic contents are not following any

specific trend. As discussed earlier,in order to investigate the impact of the current harmonic injection on force density, it is not sufficient to investigate the space and time harmonic component variation in a single position or a time instant, as the torque results from the summation of contribution of forces acting on the whole air gap line through one period of time.

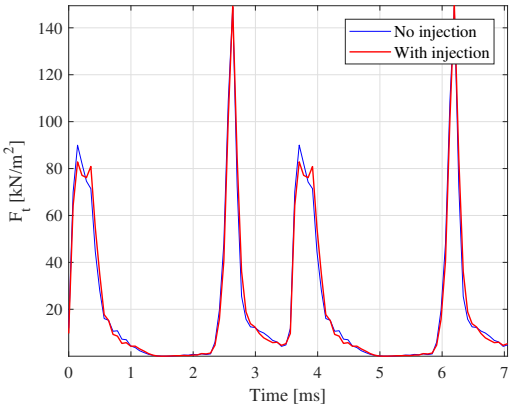

Figure 6.24: Tangential force density as a function of time before and after current harmonic injection

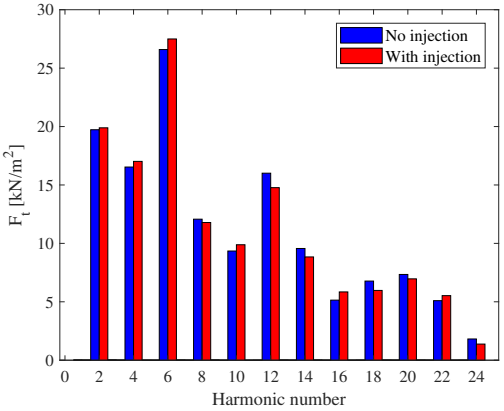

Figure 6.25: Tangential force density time domain harmonic component before and after current harmonic injection

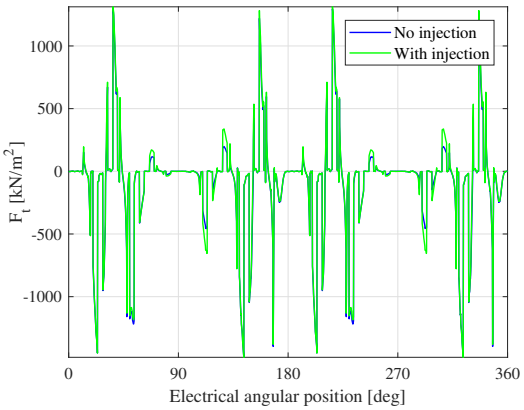

Figure 6.26: Tangential force density as a function of electrical angular position before and after current harmonic injection

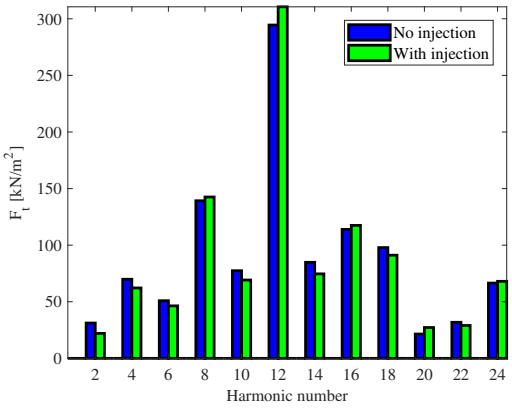

Figure 6.27: Tangential force density space domain harmonic component before and after current harmonic injection

Analytically calculating torque before and after injection of current harmonics into the current signal can give us a better understanding of changes in the force density during time, and for whole air gap, as the torque in this method is calculated

by integration of tangential force density in each time instant for the whole air gap line. As can be seen, Fig.6.28 depicts the torque calculated analytically by the use of MATLAB for normal operation for the second operating point and after injection of the $7th$ and $11th$ harmonics to the current. The harmonics in the torque determined by analytic calculation is depicted in Fig.6.29. This figure clearly shows the torque harmonic reduction after compensation, which agrees with simulation results.

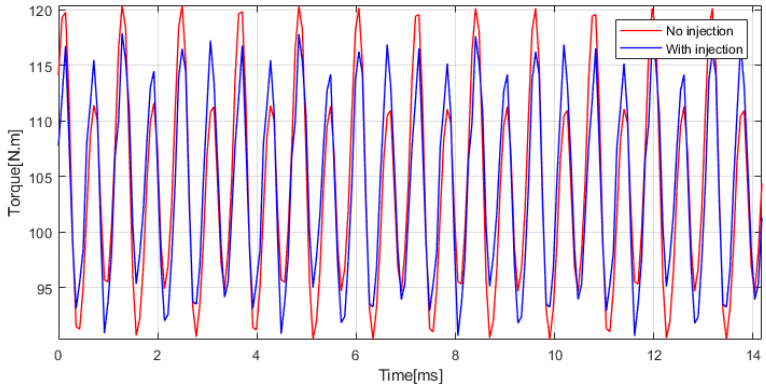

Figure 6.28: Electromagnetic torque from analytical calculation before and after current harmonic injection

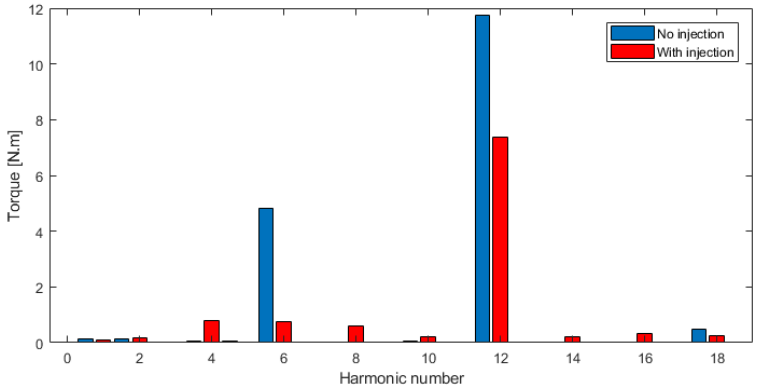

Figure 6.29: Electromagnetic torque time domain harmonic from analytical calculation before and after current harmonic injection

6.4.3 Core loss

A smoother output torque with less ripple is achieved by manipulating the current waveform as discussed before. Injecting a certain harmonic component obviously has some negative effects on losses. Here, the core losses in the PMSM is calculated and plotted by means of ANSYS Maxwell 2D. Fig.6.30 and Fig.6.31 show core losses in the stator and rotor respectively. The losses in no injection, injection of 11th harmonic component and 7th and 11th harmonic components injection to the

current is investigated and plotted. As can be seen from figures and Table.6.11, by injecting the harmonics, the core losses have been increased by almost 20 percent which correspond to a power loss of approximately 20 W.

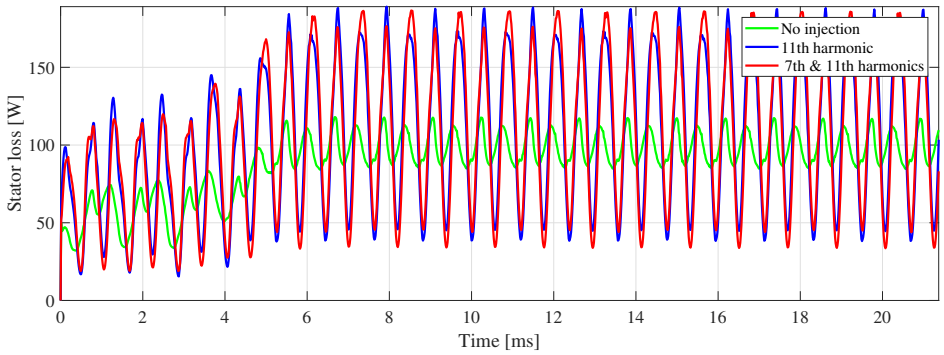

Figure 6.30: Stator core losses

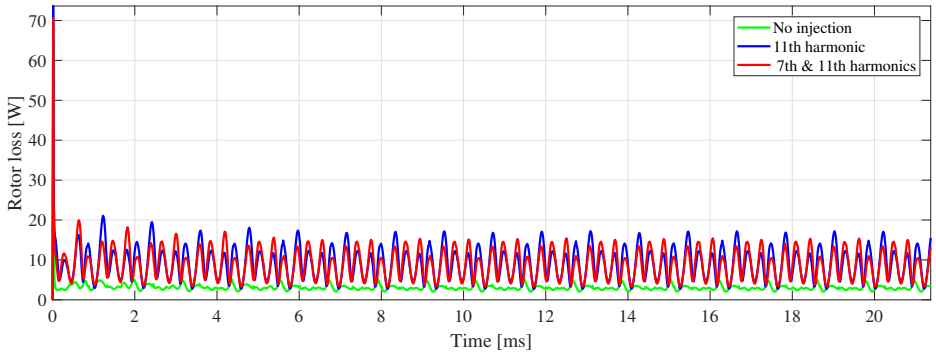

Figure 6.31: Rotor core losses

Table 6.11: Core losses in stator and rotor

Power loss	No injection	11th harmonic	7th & 11th harmonics
Rotor core loss [W]	3.01	8.95	8.76
Stator core loss [W]	98.53	115.08	114.24
Total core loss	101.54	124.03	123.01
Total core loss increase [%]	N/A	22.2	21.1

7

Conclusion and future work

7.1 Conclusion

This thesis is dedicated to a torque ripple reduction method for an IPMSM. To investigate the applicability of the method mentioned earlier, the electromagnetic forces are studied. The torque optimization is done by injecting harmonic components to the input current of the IPMSM in a way that it cancels out the effect of existing harmonics in the back EMF on the torque.

The formation of the electromagnetic fluxes and forces in the air gap of the IPMSM are investigated further in chapter 5. In addition, the analytical calculation of the electromagnetic torque from tangential forces acting on the air gap line is presented. These investigations are used to analyze the results and interpret the impact of the applied method on electromagnetic forces and consequently on the electromagnetic torque.

Table 7.1: Torque ripple enhancement in different operating points

Point	T_{Ripple} No injection	T_{Ripple} With injection	Enhancement [%]
1st point	25.5	10.5	60
2nd point	29.9	4.22	86
3rd point	27	7	74

The results obtained from the FE Modeling of an IPMSM is summarized in Table.7.1. It can be seen that in the selected operating points the torque ripple is decreased by 73% in average. It can be concluded that the applied method contributes to the desired result for all investigated operating points, but the impact size vary depending on the characteristics of the selected operating point. Although torque ripple minimization is achieved, some undesired impact on power losses in the IPMSM is observed. The core losses in the IPMSM is increased by almost 20

%. The copper losses will increase due to the harmonics in the current but its exact value is not calculated in this project. In general, the losses in the motor will increase which is a drawback of using the current harmonic injection method for torque ripple optimization.

7.2 Discussion

There are some concerns regarding the losses that may occur in an inverter due to the switching. Basically, this method is based on creating harmonics and injecting them into the current, meaning producing 5 to 13 times higher frequency current component compared to fundamental current that has to be sampled in the inverter. This could lead to a need of a high switching frequency resulting in a higher losses in the switches. On the other hand, the harmonic component size is highly dependent on the characteristics of the operating point which results in time consuming simulations or test procedures.

7.2.1 Economical, sustainable and ethical aspects

With respect to economical aspects this method is noticeably feasible as it can be conducted without any changes in the mechanical design. This means that high costs of redesigning, manufacturing of the motor and inserting expensive material can be avoided. As a result, the mining and usage of materials like iron and materials used as PMs have a potential to be reduced which in turn helps with sustaining a better environment for future generation.

Cobalt and Neodymium are essentially used in Neodymium and Samarium Cobalt magnets respectively. These magnets play an important role in manufacture electric motors. According to [24], in mining these materials human rights issues are reported. For instance, half of Cobalt's mining is done in Democratic Republic of the Congo. In this country human rights are severely violated, the mining is operated in dangerous conditions that put miner's life in danger and it is reported that miners are often children. Hence, reducing the usage of PM materials can decrease the amount of the non-ethical mining of rare earth magnets.

7.3 Future work

There are several interesting ways to continue this work to find a concrete response to the question that whether this method is applicable in a real industrial case or

not.

As mentioned, the switching losses in an inverter is a drawback with this method so the inverter behavior and switching losses can be investigated while using this method to understand if the negative effect can be acceptable or not. This can be done by sampling a current with the high frequency components or it can be investigated by co-simulating the inverter controller and the motor in a system.

Instead of injecting harmonic components into the current, they can be injected to the voltage where the voltage excitation is used to investigate the results. This is corresponding more to the real case.

To be able to implement this method in a real case, the method can be implemented in an off line mode to define a look up table which contains current references with certain added harmonics for each operating point. This may be done with smart algorithms and machine learning methods to avoid a time consuming process of testing and running simulations over and over for each operating point.

Bibliography

[1] M. Tost. Candel, "Cogging torque reduction for interior permanent magnet synchronous motor," MSc thesis, Department of Electrical Engineering and Information Technology,Technical University of Darmstadt, Darmstadt, Germany, 2016.

[2] A. Najmabadi, W. Xu and M. Degner, "A sensitivity analysis on the fifth and the seventh harmonic current injection for sixth order torque ripple reduction," 2017 IEEE International Electric Machines and Drives Conference (IEMDC), Miami, FL, 2017, pp. 1-8. doi: 10.1109/IEMDC.2017.8002209

[3] O. Josefsson, T. Thiringer, S. Lundmark, H. Zelaya, "Evaluation and comparison of a two-level and a multilevel inverter for an ev using a modulized battery topology," in 38th Annual Conference on IEEE Industrial Electronics Society(IECON),Oct 2012, pp.2949-2956.

[4] Z.Q.Zhu,L.J.Wu and Z.P.Xia, "An accurate subdomain model for magnetic field computation in slotted surface-mounted permanent-magnet," IEEE Transactions on Magnetics (2010), 110-1115.

[5] D. Casadei, F. Profumo, G. Serra, A. Tani, "FOC and DTC: Two Viable Schemes for Induction Motors Torque Control," IEEE Transactions on Power Electronic 2002

[6] Q. Wang, K. Rajashekara, Y. Jia, J. Sun, "A Real-Time Vibration Suppression Strategy in Electric Vehicles," Vehicular Technology IEEE Transactions on, vol. 66, pp. 7722-7729, 2017, ISSN 0018-9545.

[7] M. N. Ibrahim P. Sergeant E. M. Rashad "Influence of rotor flux-barrier geometry on torque and torque ripple of permanent-magnet-assisted synchronous reluctance motors," 2016 ICEM pp. 398-404 2016.

[8] Y.-K. Lin and Y.-S. Lai, "Dead-Time Elimination of PWM-Controlled Inverter/Converter Without Separate Power Sources for Current Polarity Detection Circuit," IEEE Transactions on Industrial Electronics, vol. 56, no. 6, pp. 2121 –2127, june 2009.

[9] N. Urasaki, T. Senjyu, K. Uezato, and T. Funabashi, "Adaptive dead time compensation strategy for permanent magnet synchronous motor drive," IEEE Trans. Energy Convers., vol. 22, no. 2, pp. 271–280, Jun. 2007.

[10] R. J. Kerkman, D. Leggate, D. W. Schlegel, and C. Winterhalter, "Effects of parasitics on the control of voltage source inverter," IEEE Trans. Power Electron., vol. 18, no. 1, pp. 140–150, Jan. 2003.

[11] S. Y. Kim, W. Lee, M. S. Rho, and S. Y. Park, "Effective dead-time compensation using a simple vectorial disturbance estimator in PMSM drives," IEEE Trans. Ind. Electron., vol. 57, no. 5, pp. 1609–1614, May 2010.

[12] T Wichert, "Design and Construction Modifications of Switched Reluctance Machines," Ph.D. thesis, Warsaw University of Technology,Poland, 2008.

[13] C. Hsiao, S. Yeh, J. Hwang, "A novel cogging torque simulation method for permanent-magnet synchronous machines," Energies 2011, 4, 2166–2179.

[14] W. Fei, P. Luk, "Torque Ripple Reduction of a Direct-Drive Permanent-Magnet Synchronous Machine by Material-Efficient Axial Pole Pairing," IEEE Trans. on Ind. Elec., vol. 59, pp. 2601-2611, 2012

[15] C. Schulte and J. Böcker, "Co-simulation of an interior permanent magnet synchronous motor with segmented rotor structure," IECON 2014 - 40th Annual Conference of the IEEE Industrial Electronics Society, Dallas, TX, 2014, pp. 437-442.

[16] Y. Shin1, J. Gi, M. Yoon, S. Chai, J. Hong, "Improvement of Back-EMF Waveform by adjusting Pole angle in Surface-Mounted Permanent Magnet Synchronous Machine type Generator for Fly-Wheel ," Department of Automotive Electronic Control Engineering, Hanyang University, Korea, 2015.

[17] A Andersson, "Electric machine control for energy efficient electric drive systems," Ph.D. dissertation, Department of Energy and Environment, Chalmers University of Technology, Gothenburg, Sweden, 2015.

[18] D Zarko, "A systematic approach to optimized design of permanent magnet motors with reduced torque pulsations," Ph.D. dissertation, University of Wisconsin-Madison, 2004.

[19] Staunton,R. H., Ayers, C. W. , Marlino , L. D. ,Chiasson, J. N. Burress,T. A. (2006). Evaluation of 2004 Toyota Prius Hybrid Electric Drive System. Retrieved from https://www.engr.uvic.ca/ mech459/Pub References/890029.pdf/

[20] Chapman, P.L., Sudhoff, S.D., Whitcomb, C.A., "Optimal current control strategies for surface-mounted permanent-magnet synchronous machine drives," IEEE Trans. Energy Convers., 1999, 14, (4), pp. 1043–1050

[21] Inoue, T., Inoue, Y., Morimoto, S., et al.: 'Mathematical model for MTPA control of permanent-magnet synchronous motor in stator flux linkage synchronous frame', IEEE Trans .Ind. Appl., 2015, 51, (5), pp. 3620–3628

[22] Krishnan, R. (2010). Permanent Magnet Synchronous and Brushless DC Motor Drives. Boca Raton: CRC Press.

[23] A. Walker, M. Galea, C. Gerada, A. Mebarki, and D. Gerada, "A topology selection consideration of electrical machines for traction applications: towards the freedom- car 2020 targets," in Tenth International Conference on Ecological Vehicles and Renewable Energies (EVER), March 2015, pp. 1–10.

[24] How Cobalt Neodymium Demand Impacts Magnet Pricing.(2018, March 16). Retrieved from https://www.duramag.com/techtalk/magnet-news/magnets-in-the-news-how-cobalt-neodymium-demand-impacts-magnet-pricing/